Elements of cometary aeronomy

J. F. Crifo

Centre National de la Researche Scientifique, Service d'Aeronomie, B P. No. 3, 91371 Verrières le Buisson Cedex, France

A concise but educated introduction to the physics of the gas and dust environment of comets is given. Emphasis is placed on the fact that, while the gas and dust give birth to very differing, cometary forms they are nonetheless governed by closely related processes. An effort is made to formulate these procesess with the help of the well established terminology and equations of celestial mechanics and physical gasdynamics. In doing so, we hope to convince the reader that comets, however fascinating strange objects they may appear to be, are nonetheless very orthodox solar system memebers, susceptible to be best understood by the standard methods of planatery aeronomy.

Introduction: The strange world of comets

Before discussing cometary aeronomy, a few words on comets in general may be in order. Excellent (but thick!) books covering all aspects of cometary physics have appeared in the wake of this return of comet P/Halley: the interested reader will want to consult, in particular: Grewing *et al.*[1], Mason[2], Bailey *et al.*[3] and Newburn *et al.*[4]. A more concise and very commendable tutorial account of cometary physics has been written just before the P/Halley flyby missions of 1986 by Mendis *et al.*[5]. Here, only a representative choice of topics will be discussed, and illustrated by a few references which will guide the reader to the relevant literature.

As far as we know, the definition of a 'comet' is rather flexible: it is any fast moving celestial object with changing appearance. In general, comets are observable only over a small part of their orbit. Those with orbital period $T > 200$ years are termed 'long period' comets (LPC), the others 'short period' comets (SPC) – or, currently but abusively, just 'periodic comets' (with the symbol P/ preceding the name of the SPC). By 1988, there were 644 known LPCs and about 115 SPCs. LPCs are discovered at rate 3.3 per year, and SPCs at rate 0.25 per year. Cometary orbits are generally changing with time, due to the perturbing effects of the giant planets. Sometimes the change is so important that the comet is lost from the inner solar system: therefore, some of the newly discovered comets must actually be 'new' comets, to balance the preceding loss.

Far from the Sun, most comets are point-like, and their brightness is interpreted in terms of cross-section of a solid-object, the 'nucleus'. Assuming a visible albedo of 0.03 for the nucleus, the range of observed comet nucleus photometric radii is $1.25 < R_n < 12.5$ km, but two larger objects are known: P/Schwassmann–Wachmann ($R_n \simeq 20$ km) and Chiron ($R_n \simeq 100$ km).

The total number of comets 'present' (i.e. having momentarily an orbit with low perihelion) in the inner Solar System can only be guessed, since many 'small' comets, and many comets with unfavourable orbits (from the point of view of visibility) certainly escape detection. It has been estimated that, in the precedingly mentioned nucleus size range, there probably exist $\simeq 350$ SPC with perihelion within the orbit of Jupiter, about 1/3 of which only have already been discovered; the corresponding estimate for the LPC family is five times greater![6]

Closer to the Sun, comets assume a fuzzy appearance (the 'coma'), due to the apparition of dust and gas around the nucleus; 33 comets have been observed with a coma beyond 5 AU (see note 1), four of which still having one at 10 AU[7]; but, in general, the coma develops near 3 AU, and it is also in general at this distance that appears a group of molecular emission bands from the coma; in the visible, the most conspicuous ones are, bizarrely enough, due to the carbon clusters C_2 and C_3 and to the radical CN! Also currently observed are bands of NH_2 and the forbidden red lines from $O(^1D)$.

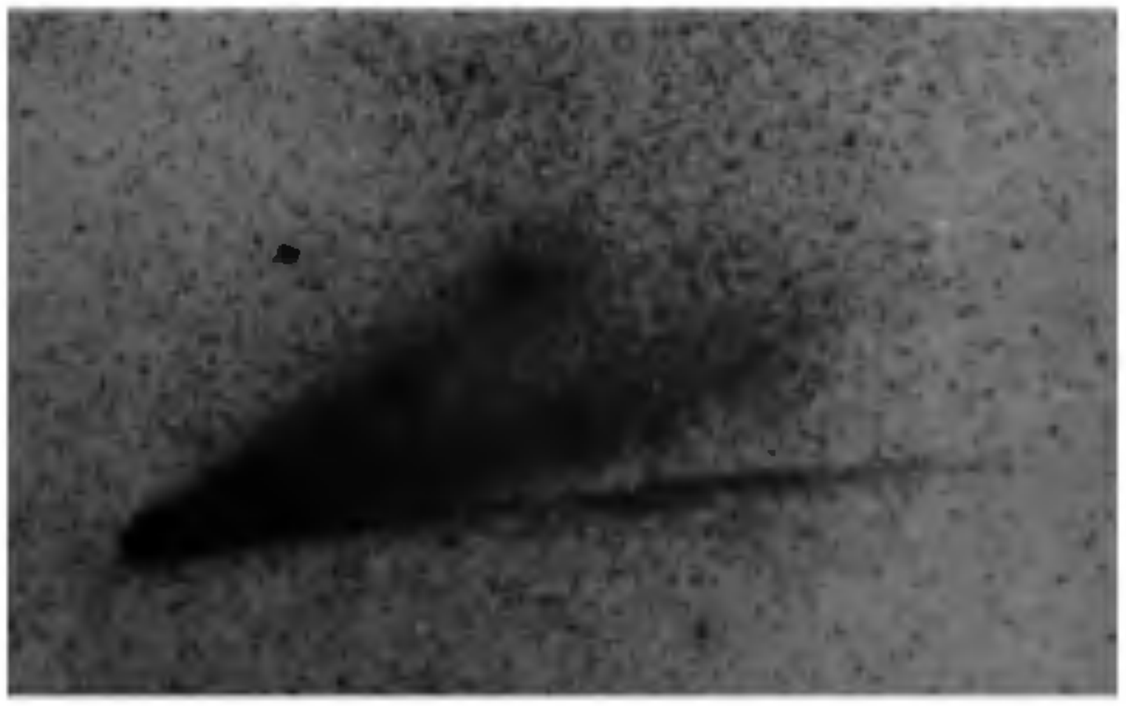

Figure 1. The two tails of comet Kohoutek (courtesy S. Koutchmy)

Table 1. A list of identified cometary gas-phase species In no comet has the full list been detected, and the indicated abundances are representative only (however, there is no objection against the presence of all these species in any comet) We have omitted from the Table the many metals and metallic ions reliably observed in Sun-grazing comets (e g Na, K, Ca, Ca^+, Fe ..) and molecules for which only one identification has been published (e g S_2, CO_2) The year is that of first *definitive identification*, not that of first observation Most values of β_{ph} are subject to a large uncertainty, for H, β_{ph} is negligible with respect to the solar wind destruction rate β_{SW} which is of order $7\ 10^{-7}$ at 1 AU

Atomic mass	Stable molecule	Radical	Molec ion	Radical ion	Typical abundance	β_{ph} (1 AU) s^{-1}	Year
1		H			–	$7\ 3\ 10^{-8}$	1970
12		C			0 1–0 2	$4\ 1\ 10^{-7}$	1974
				C^+			1976
13		CH			0 007	$1\ 2\ 10^{-2}$	1940
				CH^+			1941
15		NH			0 0002	$2.5\ 10^{-6}$	1941
16		NH_2			0 003	$3\ 0\ 10^{-5}$	1943
		O			–	$7.1\ 10^{-7}$	1974
17		OH			–	$9\ 0\ 10^{-6}$	1941
				OH^+	–		1950
18	H_2O				0 8	$1\ 2\ 10^{-5}$	1986
			H_2O^+		–		1974
19				H_3O^+	–		1984
24		C_2			0 003	$1\ 0\ 10^{-6}$	1882
26		CN			0 003	$4\ 0\ 10^{-6}$	1882
				CN^+			1980
27	HCN				0 001	$1\ 5\ 10^{-5}$	1974
28	CO				0 1	$6\ 7\ 10^{-7}$	1976
			CO^+				1910
			N_2^+		0 0002		1910
30	HCHO				0 005	$2\ 0\ 10^{-4}$	1986
32	CH_3OH				0 01	$1\ 3\ 10^{-5}$	1991
		S			0 01		1980
34	H_2S				0 002	$3\ 0\ 10^{-4}$	1991
36		C_3			0 0002	$1\ 0\ 10^{-5}$	1954
44		CS			0 001	$2\ 0\ 10^{-3}$	1976
44			CO_2^+				1950

At varying distances from the Sun, most comets develop several (one to three) types of tails (see Figure 1). The *ion tail* is a straight narrow beam of molecular ions, the emission bands of which give it distinct colours; it is nearly exactly antisolar, and is the seat of many dynamical processes: fast ($\simeq 10^2$ km/s) motions of denser regions, and sometimes spectacular tail breakup. The *dust tail* is broad, fan-shaped and only roughly antisolar; it has the solar colour characteristic of dust scattering. On rare occasions, the dust tail is observed edge-on and projects itself on the sky both behind and in front of the comet: the resulting *apparent* sunward spike has long improperly been believed to constitute a third type of tail. The typical size of a dust tail at 1 AU is 10^7 km. The visible (dust) coma extends typically to 10^4 km, and the extent of the gas coma depends upon which species is observed: the greatest one is that of atomic hydrogen H, typically 10^5 km: the largest object in the Solar System!

At this time (mid-1991), 27 molecules, radicals and ions have been reliably identified in comas using observations at visible, UV, IR and radio wavelengths (see Table 1). There is all evidence that such a list is incomplete, as shown by P/Halley *in situ* mass spectra, by the existence of unidentified spectral bands, and by theoretical chemical modelling; however, the most abundant species are probably all in the table. Among the most frequently suggested unobserved (minor) species are CO_2, N_2, NH_3, CS_2, and a wealth of organic molecules.

Consideration of the list of species identified by 1950, and cosmic abundance arguments, led Whipple[8] to suggest that comet nuclei were 'a matrix of meteoritic material... mixed together with frozen gases [which, furthermore] constitute an important, if not a predominant fraction of the mass'. The cometary activity would then be driven by solar light-induced sublimation of these ices (see note 2). The sublimation

of the least volatile of these ices, H_2O ice, satisfactorily provides an activity onset near 3 AU, and it was thus presumed to be the dominant ice. This conjecture was spectacularly enforced by the discovery of the huge atomic H coma, and, much later, by that of H_2O itself as the dominant coma molecule: this was achieved in 1986, on P/Halley, (i) from the Earth by high resolution IR spectroscopy[9], (ii) *in situ* by the neutral mass spectrometer of the 'Giotto' spacecraft[10], and (iii) from the comet vicinity by the infrared spectrometer of the Soviet *Vega* spacecraft[11]. However, direct detection of *ice* itself is still missing. In any case, ice sublimation cannot explain the activity of many comets far outside of 3 AU, and there is evidence that comet nuclei are quite inhomogeneous: Whipple's model does not tell us everything about comet nuclei!

The gas production rates Q_g of observed comets at 1 AU from the Sun are in the range $3.10^{27} \leq Q_g \leq 10^{30}$ mol/s[12]. If H_2O production is a consequence of ice sublimation, it should vary in proportion to the solar flux, i.e. as r_h^{-2} for r_h, the heliocentric distance, smaller than $\simeq$3 AU (see note 3). This dependence seems roughly verified for $r_h < 2$ AU but the issue is unclear beyond this distance[12].

The question of how much dust is emitted is not easy to answer. Dust is observed via scattering in the visible, and via thermal emission in the infrared. In both cases, the brightness peaks at wavelengths comparable to the grain size. Therefore, one currently measures the loss rate in *small* grains only (say with typical size 0.1 to 20 μm). This represents typically 0.5% to 50% of the water mass loss[12]. Various lines of evidence, and in the first place the *in-situ* results from the European 1986 P/Halley flyby spacecraft *Giotto*, suggest that much higher mass loss occurs via large grains (up to decimeter size).

In spite of these rather well characterized general properties, every comet has its own history and peculiarities, involving sometimes such hectic events as strong outbursts (over 12 comets), fading and disappearance of the comet before perihelion, and nucleus splittings (21 comets) (see Hughes[13]) (see note 4). Nonetheless, there is no compelling evidence against considering all comets as members of a homogeneous physicochemical group (aside from surface modifications resulting from their solar irradiation near perihelion).

The understanding of cometary nuclei is the ultimate goal of the study of comets, because they are small bodies spending most of their life in very cold places: therefore, they may carry unaltered information on the remote past of the Solar System, otherwise obliterated in large and/or in hot bodies by internal reprocessing ('differentiation'). However, the prospects for future direct experimentation on comet nuclei are not encouraging: for at least a decade, only the coma will remain observable. At the present time, practically all data on comas refer to regions with distance to the nucleus in excess of 1000 km (this being true even in the case of the 1986 flybys of P/Halley!). Future improvements of the spatial resolution of ground-based observations, and even close *rendezvous* with a periodic comet (ESA Project 'ROSETTA') will hopefully provide access to much closer distances to the surface. This context legitimates the patient development of state-of-the art models of the comas, that would be comparable to what is achieved for planetary atmospheres. But, there are also other strong incentives for the construction of comprehensive coma models: (i) such a task is a challenge to theoretical Rarefied Gas-Dynamics, because it implies consideration of all flow regimes from inviscid to free-molecular; (ii) it is a fascinating exercise in comparative aeronomy, because it involves solid bodies with sizes from km to hundred km; (iii) it is a challenging task for physical chemists as well because it involves the properties of molecules under cold and non-equilibrium conditions. Here, after a brief summary of the presently meagre knowledge of comet nuclei, we will devote about equal space to the physics and chemistry of the inner, little observed coma, and to the physics of the currently observed outer collisionless coma. Emphasis will be placed on the dynamical processes, more than on the radiative emission processes, because the former are more essential to the understanding of the cometary atmospheres. Unfortunately, we will almost completely omit discussion of the most interesting plasma processes, because this would have duplicated, at the least, the length of this study.

Physical properties of Comet nuclei

The only direct observation of a cometary nucleus consists in multicolour pictures of P/Halley nucleus taken from the 1986 flyby spacecrafts. P/Halley is historically famous because in an attempt to verify Newton's conjecture that all Solar System bodies including comets move on conic sections, E. Halley in 1705 pointed out probable past observations of this comet, and predicted its return for the end of 1758. He unfortunately died before this prediction was spectacularly confirmed.

P/Halley is a somewhat unusual SPC, retrograde, very active, and with a long period of 76 years; it was near 0.9 AU from the Sun during the 1986 flyby observations. Figure 2 summarizes the appearance of its nucleus, and also indicates the probable direction of the spin axis S and angular momentum axis[14] M. According to reference 14, the comet spins around S in 2.84 days, and S precesses around M in 3.69 days. These rates are typical of the few comets for which a spin rate can be guessed. Incidentally, the authors note that P/Halley's

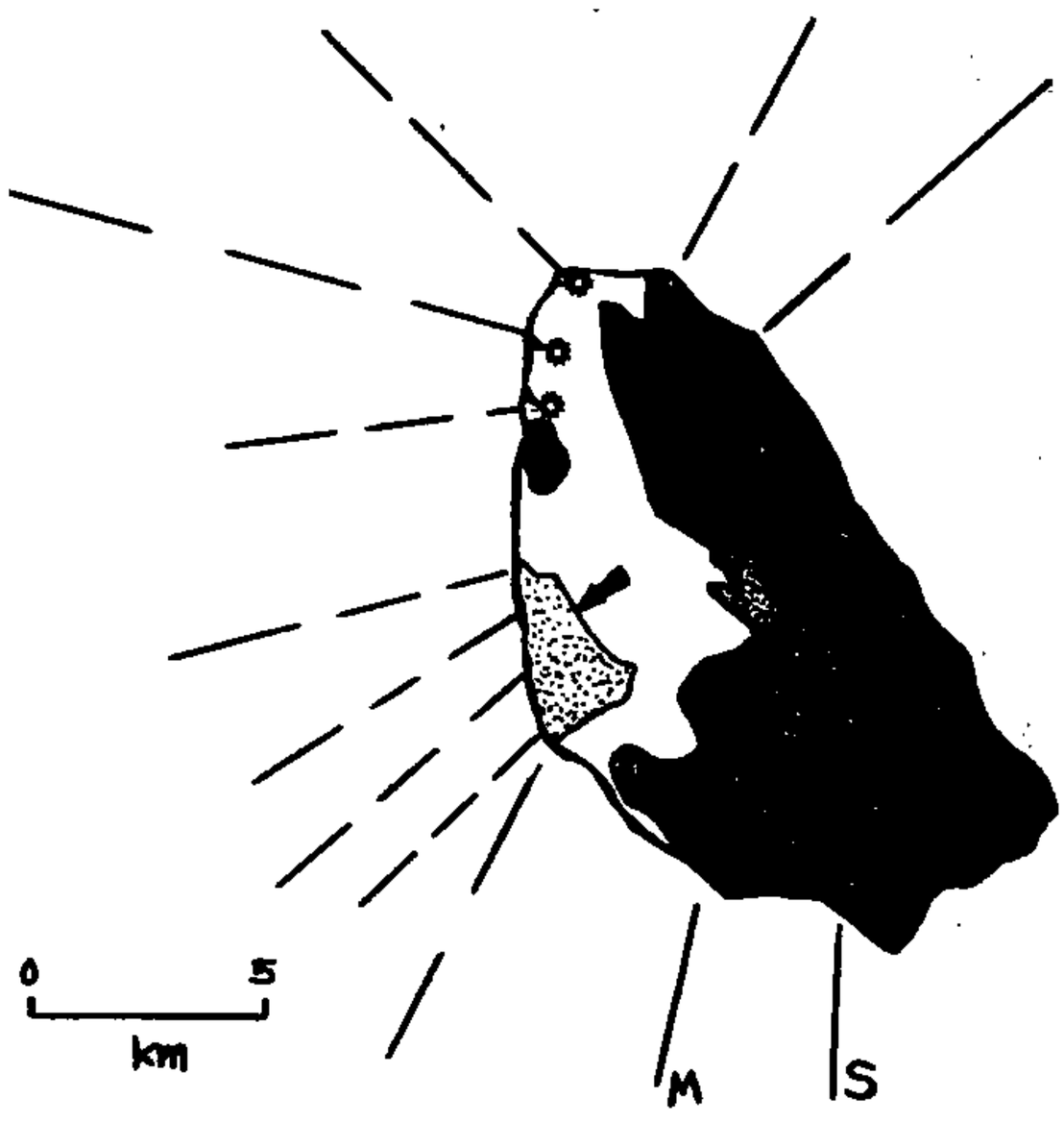

Figure 2. P/Halley's nucleus (after Keller *et al*[50], and Belton *et al*[14]). The Sun direction is to the left, 27° above the horizontal, and 15° behind the drawing plane. The main directions of emission or dust are indicated by dashed lines. The M and S axis are related to the nucleus rotation (see text). The arrow distinguishes the area presumably responsible for the CN features in the coma.

spin state is not the minimum allowed for its angular momentum: this may indicate that many minor splittings and/or one large splitting occurred in the recent past of this comet.

The dust apparently issues very unevenly from this nucleus as indicated in Figure 2: only a total area $A_{eff} \simeq 3.4\ 10^{11}$ cm^2, representing about 10% only of its external surface is dust-emitting. As regards the gas, only inferences can be made: the radial distribution of the most abundant molecules H_2O and CO beyond 1000 km suggests spherically symmetric emission, but consideration of the balance between solar energy and sublimation latent heat suggests emission from an active area similar in extent to the dust-emitting area. The existence of well-defined periodic fluctuations in the production of C_2, C_3 and OH also suggests discrete production sites, as does the observation of spiral structures in the distribution of the radical CN; the attempt of Belton *et al.*[14] at providing a consistent account of these effects led them to the assumption of five discrete emitting areas with differing chemical properties, one of them only being responsible for the CN spiral features (see Figure 2).

The visible and IR spectrophotometry of the nucleus performed from the flyby spacecrafts revealed that, on the average, the nucleus is very dark (albedo of a few %) and hot (350 K). This is clearly incompatible with a dominantly icy surface, but does not exclude the presence of ice in the active regions.

To our knowledge, there is just no information of any kind concerning the chemical composition of P/Halley's nucleus: all one can say for sure is that it stores under some form the material observed in the coma!

Finally, it is important to figure out what a nucleus mass M_n (or average density ρ_n) may be. Here again, P/Halley offers the most reliable case for an estimate. Its observed nucleus volume is $\simeq 550$ km^3, corresponding to an effective radius (see note 5) $R_n = 5.1$ km. For ρ_n, an unbiased assessment yielded the large uncertainty $0.03 < \rho_n < 4.9$ g cm^{-3} (ref. 15). In the following, we take $M_n = 3.10^{17}$ g.

From all this, we may retain that P/Halley's nucleus has a complex shape, and is physically and chemically inhomogeneous. Similar conclusions based on the morphology of dust emissions have been arrived at for several other comet nuclei by Sekanina[16]. One may also assume this nucleus to be well representative, including in size, since it is about at the middle of the range of measured nucleus sizes.

Finally, let us indicate that there is a vast literature on what we could call 'possible properties of comet nuclei', and even costly laboratory projects aimed at reproducing these possible properties. We refer the interested reader to Newburn *et al.*[4].

Physical conditions in cometary atmospheres

The word 'atmosphere' itself refers to the fluid environment of a solid body. For planets and stars, the confinement of the atmosphere against vacuum outflow is ensured by body forces (gravity and/or magnetic fields). Such atmospheres are essentially static, with first-order dynamical effects. In comets, gas molecules quit the nucleus with thermal velocities at nucleus surface temperatures in the range 30–300 K. For simple molecules, these velocities V are in the range 0.1 to 1 km/s, much in excess of typical nucleus escape velocities $V_{esc} = (2GM_n/R_n)^{1/2} \simeq 7.5\ ^{10\text{-}4}\ R_n(\rho_n)^{1/2}$, which are of a few m/s. Thus, gravitational confinement is totally excluded. It would be surprising also to discover a strong magnetic field around such a small and cold object as a comet nucleus; indeed, the *Giotto* spacecraft has set an upper limit of 1 nT to the magnetic field within a cavity of $\simeq 5000$ km around P/Halley's nucleus. Therefore, no *static* neutral or ionized atmosphere can exist around a comet nucleus (see note 6). At best, a *stationary* atmosphere in steady outflow can be maintained for periods of time where the nucleus emission is stationary. Limits on the duration of stationary conditions are set by the rate of change of the heliocentric distance and by the nucleus rotation rate:

observation reveals that comas are nonetheless currently quasi-stationary. Here, we will not discuss the transient phenomena (outbursts, etc.).

The most complete description of an atmosphere is provided by the phase space densities, or distribution functions (d.f.), $f_i = dN_i/d\Gamma$, of all its constituents (i): dN_i is the number of particles per elementary *phase space* volume $d\Gamma_i$. The d.f. are governed by Boltzmán's equations, which, in general, cannot be solved. An exception is the collisionless case. Most observations of comets indeed concern the outer regions of the atmosphere, the observable coma, in which collisions, are rare or absent. But the in-depth understanding of these observations, that is their extrapolation in terms of nucleus properties, requires the detailed modelling of the unobserved inner regions, where collisions play a dominant role.

In a collision-dominated atmosphere, the determination of the f_i's must be abandoned in favour of that of a restricted number of their velocity space moments (mass density, flow velocity, temperature, ...). The number of moments to consider depends upon the extent to which the collisions keep the d.f. in a state not too far from the thermal equilibrium Maxwell–Boltzman form. This question has been studied in very great detail in the Rarefied Gas Dynamic context. The key parameter to consider is the 'Knudsen number' $K_n = \Lambda/R$, where Λ is the gas mean-free path, and R the smallest scale over where the properties of the atmosphere vary. It is now well established (see e.g. chapter 15 of McCourt *et al.*[17] that (i) one can use, for $K_n \leq 0.1$ the inviscid (or 'five moment') Euler equations; (ii) for $0.1 \leq K_n \leq 10$ (the so-called transition regime) the Navier–Stokes equations and/or a choice of approximate but manageable Boltzman equations; and (iii) for $K_n \geq 10$ the collisionless Boltzman equation (or Liouville equation).

In a static atmosphere, hydrostatic equilibrium prevails, whereby the density decreases about exponentially with radial distance r. Therefore, the transition between fluid and collisionless regions is abrupt (a few atmospheric scale heights), and one can ignore the transition regime and define a 'collisionopause' separating the inviscid region from the collisionless region. In the case of a spherically outflowing atmosphere, however, the density n_g decrease follows about an inverse square law; the characteristic flow scale, $R = n_g/|dn_g/dr| = r/2$ and $\Lambda \propto 1/n_g \propto r^2$, so that $K_n \propto r$: the transition regime affects a much larger coma volume than the inviscid region, and it is not possible to define any 'collisionopause' in the preceding sense.

As a numerical example, we may choose P/Halley's coma at the time of the flyby observations. Water was emitted at a rate $Q_g = 7.10^{29}$ mol/s from A_{eff}; assuming an initial radial velocity $\simeq 0.3$ km/s an initial flow scaling length $R_n^{eff} = (A_{eff}/\pi)^{1/2} = 3.3$ km and the H_2O 'effective hard-sphere cross-section' given in Crifo[18]:

$$\sigma_{H_2O}(T) = 1.66\,10^{-15}(T/300)^{-0.6}\ \text{cm}^2 \qquad (1)$$

one gets $K_n^0 = 5.10^{-6}$ (see note 7). With an inverse square decrease of the gas density, the inviscid region thus extends out to $\simeq 500$ km, and the transition regime region out to $\simeq 5000$ km. It is interesting to compare this with the result from the direct Monte-Carlo simulation of this coma by Hodges[19], reproduced in Figure 3: one sees that the H_2O d.f. starts to depart from its equilibrium form at 10^4 km. The large difference between this result and the preceding estimate is perhaps due to the fact that Hodges uses for H_2O–H_2O collisions a potential which is not consistent with the empirical cross-section (1).

The collisional coma

The preceding considerations are applicable to a homogeneous fluid. A mixture of differing constituents constitutes a single fluid to the extent that mutual equilibrium prevails among them, i.e. that they share a common temperature and flow velocity and comply with the laws of chemical, radiative, and interphase equilibrium. It is then possible to compute the hydrodynamic evolution of the fluid in terms of 'effective' physical properties (e.g. specific heats) derived from mixing rules. The surface erosion of a comet nucleus, however, is a violent event, which most probably does not produce a mixture of gas and solids in mutual equilibrium. Furthermore, the solar illumination is a source of disequilibrium, by, for instance, introducing temperature differences between grains, and seeding the gas phase with chemically reactive and dynamically fast radicals. An example of this is visible in Figure 3: the daughter molecules H and OH not only cease to be in equilibrium with H_2O beyond 10^3 km, but they also cease to attain internal thermal equilibrium beyond this distance.

Under such circumstances, it may happen that no fluid approach is possible at all, leaving Monte-Carlo simulations as the only modelling tool. However, it may also happen that some constituents or subsets of constituents have mutual interactions (collisions or long-range interactions) sufficiently efficient to keep them in or not too far from *partial* thermal equilibrium: that is, their d.f. will be not too far from a *drifting* Maxwellian. In such a case, one can consider these constituents as forming a single fluid with its own temperature and velocity. The other constituents may be fully out of equilibrium, or may also form fluids with distinct velocity and temperature: one comes out with a 'multifluid' description of the medium. Of course, these fluids are not fully isolated from one another:

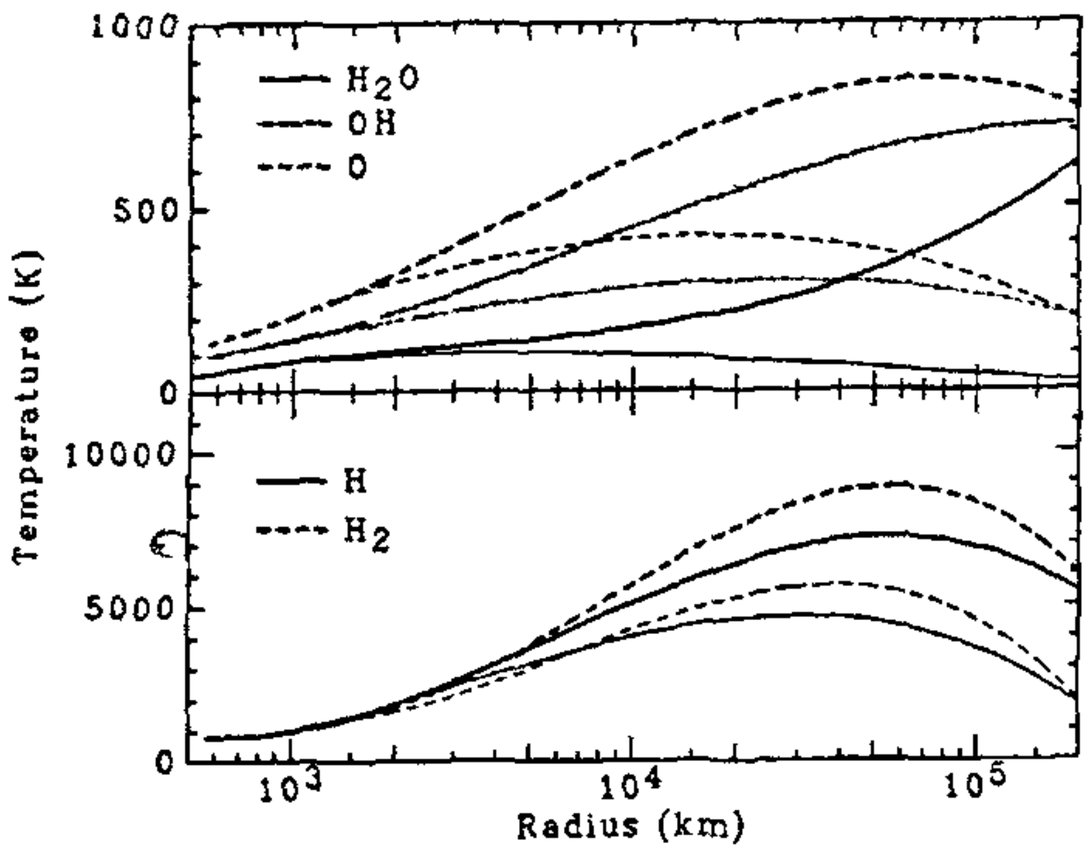

Figure 3. Full Monte-Carlo simulation of P/Halley's coma[19] The simulated species velocity distribution is approximated by a drifting ellipsoidal distribution, with axis aligned on the vertical to the nucleus the heavy lines show the corresponding parallel temperature, and the thin lines the perpendicular temperature

interactions exist between the constituents of differing fluids, so that, if sufficient time were available, global equilibrium would finally be reached. Therefore, the equations governing the different fluids will be coupled via terms allowing for the dynamical and/or chemical interactions between the fluids.

The basis for the construction of a multifluid description is the systematic evaluation (not always easy!) of the time constants $\tau^{d_j}_{d_i}$ for attainment of equilibrium between the degree of freedom (d_i) of constituent (i) and the degree of freedom (d_j) of constituent (j). Some application of this method in the case of a coma is done in Mendis *et al.*[5] At the present time, however, no canonical multifluid description of a coma has yet emerged. Depending upon the context in which a model is developed, the approach differs (see Crifo[20]). The list *of the fluids which have been considered (not all in the* same model) is: (1) H_2O pure or mixed with other neutrals and/or ions; (2) 'thermal' H atoms; (3) 'fast' H atoms; (4) neutral water clusters $(H_2O)_n$; (5) dust grains; (6) electrons (see note 8); (7) ions.

It follows from the preceding discussion that the definition of 'the' fluid region in a coma depends upon which subset of constituents is considered, since at the same point can possibly coexist fluids in inviscid, transition, and collisionless regime (see note 9). Here, we define the fluid region as the region where $K_n \leq 10$ for the *most abundant* species, H_2O. The present coma observations yield only very limited information on the physics and chemistry of this region; H_2O itself is observed only under exceptional conditions. Thus one has up to now evaluated the dominant processes on the basis of simplified models only. In the first place, the geometry of flow (so difficult to treat, from a numerical analysis viewpoint) is oversimplified: most generally, *spherical outflow from a spherical nucleus is assumed* (see note 10).

In zero-order approximation (the so-called adiabatic approximation), the vacuum expansion of a fluid is characterized by an increase of the radial gas velocity (due to the pressure gradient), therefore by a decrease in gas temperature (for energy conservation) down to negligibly small values. Accordingly, the distant expansion is supersonic. The distance from the source at which the sonic point is crossed depends upon the expansion geometry: for instance, in a converging–diverging nozzle this occurs at the throat; for strong adiabatic sublimation, this occurs within a few mean-free paths from the surface of the ice.

In the next order of approximation, one needs to consider a wealth of non-adiabatic effects: (i) energy can be lost by thermal emission or gained by absorption of external radiation in the regions where the fluid is rarefied enough to become optically thin in certain regions of the spectrum; (*ii*) the fluid can be heated by chemical processes which occur inside it; (iii) if the fluid is part of a multifluid flow, interactions with the other fluids generally lead to net energy exchanges: for instance, in the case of the inner coma, gas and dust energy exchanges must be considered. If one allows for these three effects, he obtains for spherically symmetric outflow of cometary H_2O an 'S' shaped vertical profile with a pronounced minimum in the 10 K region, followed by a strong maximum ($\simeq$ 300 K or more)[5, 23, 24]. The flow starts sonically from the surface, except if *there is a large fraction of fine dust, in which case the* sonic point is reached at a small distance from it[25].

The preceding list of adiabatic effects is however incomplete: it does not allow for the fact that water is a *condensible* vapour – the most classical example of a condensible vapour! Strong cooling of water vapour *never* leads to the obtention of very cold vapour, but to a 'fog', that is, to a mixture of vapour and droplets (or of vapour and snowflakes). The main consequence is a drastic alteration of the temperature profile of the coma, including, possibly, the establishment of a stationary recondensation shock, followed by a second sonic transition.

In the following, we give first, a general description of the transport equations that govern the evolution of the *coma fluids, and then give some indications on the main* rate equations that govern the evolution of the fluids' internal degrees of freedom. We discuss only neutral (or weakly ionized) fluids, which can be considered to expand *in a vacuum*. The case of charged coma fluids is much more complicated, for two reasons at least: (i) their fluid behaviour is preserved to any distance of

interest, i.e. out to within the plasma tail; (ii) these fluids do not expand in a vacuum, but within another supersonic fluid, the Solar Wind: a wealth of discontinuity surfaces structures their interaction with it. For an introduction to this problem, see Mendis *et al.*[5], and for a recent review see Cravens[26].

General multifluid equations

For the sake of generality, we write the full Navier–Stokes equations which express the budget of mass, momentum and energy of a fluid element undergoing spherically symmetric flow:

$$\frac{\partial \rho_i}{\partial t}+\frac{1}{r^2}\frac{\partial}{\partial r}\left(r^2 \rho_i V_i\right)=\sum_j \dot{M}_{i,j}, \tag{2}$$

$$\begin{aligned}\frac{\partial}{\partial t}\left(\rho_i V_i\right)+\frac{1}{r^2}\frac{\partial}{\partial r}\left(r^2 \rho_i V_i^2\right)+\frac{\partial p_i}{\partial r}\\ -\frac{4}{3}\mu_i \frac{\partial}{\partial r}\left(\frac{\partial V_i}{\partial r}+2\frac{V_i}{r}\right)-F_i\\ =\dot{\Pi}_{i,r}+\sum_j\left(\dot{\Pi}_{i,j}+\dot{M}_{i,j}V_j\right),\end{aligned} \tag{3}$$

$$\begin{aligned}\frac{\partial}{\partial t}(\rho_i e_i)+\frac{1}{r^2}\frac{\partial}{\partial r}\left\{r^2\left[(\rho_i e_i+p_i)V_i-\kappa_i\frac{\partial T_i}{\partial r}\right]\right\}\\ +\frac{4}{3}\ddot{\mu}_i\left\{\frac{V_i}{r}\frac{\partial V_i}{\partial r}-\left(\frac{\partial V_i}{\partial r}\right)^2\right\}-F_i V_i\\ =\dot{E}_{i,r}+\sum_j(\dot{E}_{i,j}+\dot{\Pi}_{i,j}V_j+\dot{M}_{i,j}V_j^2/2),\end{aligned} \tag{4}$$

where ρ_i is the mass density, e_i the specific energy density, μ_i the shear viscosity, κ_i the heat conductivity coefficient, F_i a macroscopic force term, and where the dotted quantities at the r.h.s. are non-conservative terms representing the budget of mass ($\dot{M}$), momentum ($\dot{\Pi}$) and energy ($\dot{E}$) exchanges with radiation – subscript (i, r) – and with the other fluids – subscript (i, j) –, or of internal processes within the fluid itself – subscript (i, i).

For a 'perfect gas of polyatomic molecules with molecule mass m_i and an intermolecular interaction potential $\propto r^{-\nu_i}$' one has:

$$p_i=\rho_i k_B T_i/m_i;\quad e_i=r_i/(\gamma_i-1)(k_B T_i/m_i)+V_i^2/2, \tag{5}$$

$$\mu_i=5C(\nu_i)T_i^{2/\nu_i}(m_i k_B T_i/\pi)^{1/2}, \tag{6}$$

$$\kappa_i=(75/4)C(\nu_i)T_i^{2/\nu_i}\,k_B(k_B T_i/(\pi\, m_i))^{1/2}, \tag{7}$$

in which γ_i is the ratio of specific heats, k_B Boltzman's constant, and $C(\nu)$ a constant obtained by a proper collision integral.

The evaluation of the r.h.s terms $\dot{M}$, $\dot{\Pi}$ and $\dot{E}$ requires solving not only the preceding hydrodynamic equations for all fluids, but, in addition, the so-called rate equations which govern the evolution of the *internal* degrees of freedom of each fluid: examples of such internal degrees of freedom are: the mole fraction of chemical species, the populations of rotational and vibrational levels of the molecules, the dust grain internal temperature. Rate equations may be avoided only for those degrees of freedom which achieve sufficiently fast equilibration at the fluid temperature.

Radiative processes

Detailed modelling of the emission and absorption of radiation by cometary molecules is needed to fit high spectral resolution data, and to evaluate the $\dot{E}_{i,r}$ terms. In the collisionless coma, one deals with pure fluorescent excitation, and the coma is generally optically thin to all wavelengths of interest. In the fluid region, however, collisional excitation and de-excitation (quenching) compete with fluorescent excitation, and optically thick conditions may prevail. If the rates of collisionally induced transitions exceed all other absorption and emission rates, local thermal equilibrium (LTE) holds. This may happen in the innermost coma, but it is clear that as the density decreases, this will cease to hold. The modelling of the excitation of cometary molecules thus requires a kinetic approach. The relative population P_j^i of any energy level (j) of any internal degree of freedom (i) (e.g. rotational) of a molecule in a fluid, obeys the equation:

$$\begin{aligned}\frac{\partial P_j^i}{\partial t}+\frac{1}{r^2}\frac{\mathrm{d}}{\mathrm{d}r}(r^2 P_j^i V_i)=\sum_j\left[K_{j',j}^i(T_i)P_j^i-K_{j,j'}^i(T_i)P_j^i\right]\\ +\sum_{j'>j}P_{j'}^i A_{j',j}^i-\sum_{j'<j}P_j^i\,A_{j,j'}^i+\sum_{j'\neq j}(B_{j',j}^i P_{j'}^i-B_{j,j'}^i P_j^i)u(\lambda_{j,j'}^i),\end{aligned} \tag{8}$$

where $K_{j,j'}^i$ is the rate of collisionally induced transition ($j\rightarrow j'$), $A_{j,j'}^i$ and $B_{j,j'}^i$ the Einstein coefficients for spontaneous and induced emission, $\lambda_{j,j'}^i$ the wavelength of the transition, and $u(\lambda)$ the coma radiation density. These equations must be coupled to radiation transfer equations for u, insofar as the inner coma is not necessarily optically thin to all wavelengths[24]. This theory has been applied to cometary H_2O by Bockelee-Morvan *et al.* who succeeded in fitting remarkably well the rotational spectrum of P/Halley water obtained by an airborne interferometer by Weaver *et al.*[9] (see Figure 4). A similar theory has been

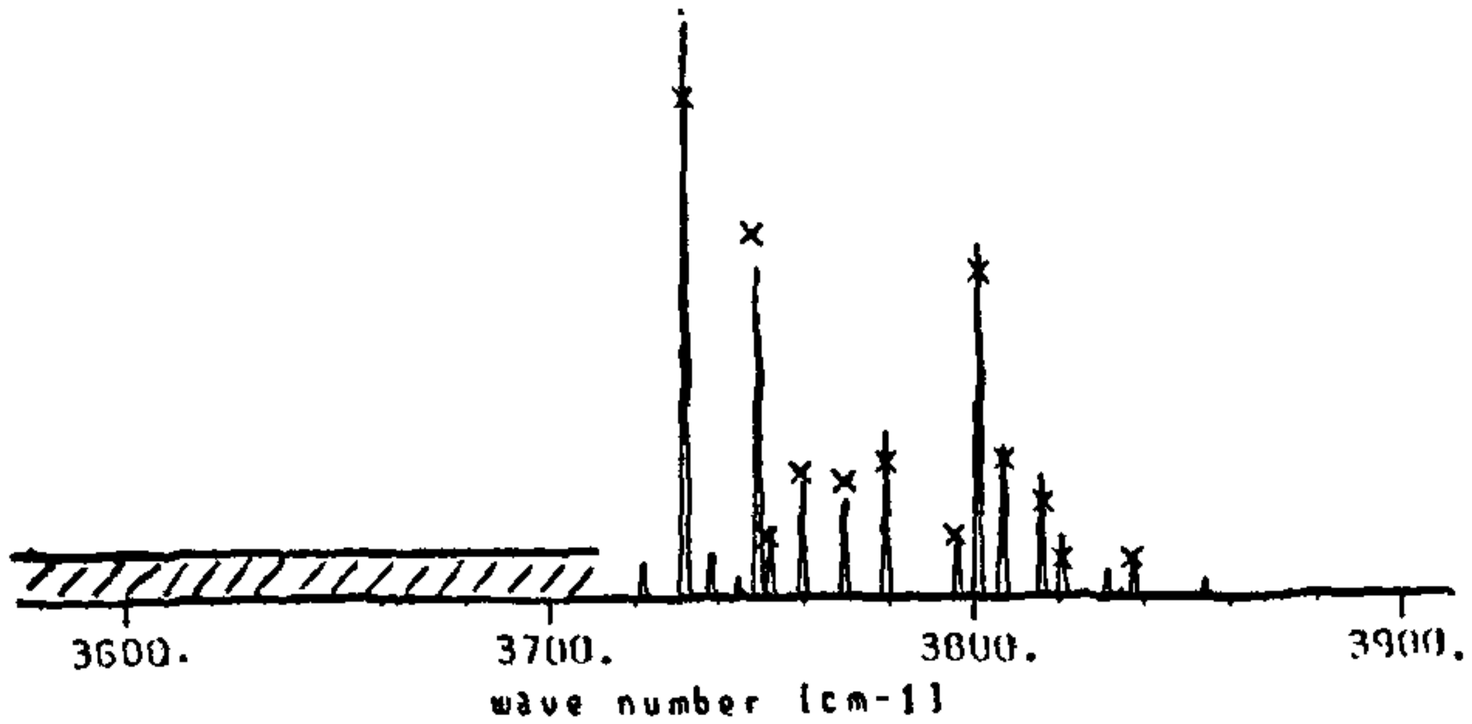

Figure 4. Rotational emission of H_2O in P/Halley, from Bockelée Morvan and Crovisier[51]. Crosses indicate the line positions and relative intensities of the observations of the ν_3 band of water of Weaver *et al*[9], and the continuous line is a model emission spectrum based on an excitation model. The hatched region was not observable.

developed for other presumably 'primary' molecules, e.g. CO (ref. 27).

Due to the collisional excitations and de-excitations, and to the small optical thickness of the coma, kinetic energy can be transformed into internal molecular excitation energy (rotational, vibrational, . . .) and vice-versa. The effect is represented fully by inserting in equation (5) the value $\gamma_i = (\delta_i + 5)/(\delta_i + 3)$, with δ_i the number of internal degrees of freedom *in* LTE, and by setting in equation (4)

$$\dot{E}_{i,r} = \rho_i \sum_{i_k} \sum_{j'>j} (P'^{i_k}_{j} K'^{i_k}_{jj'} - P'^{i_k}_{j'} K'^{i_k}_{j'j}) hc / \lambda'^{i_k}_{jj'}, \qquad (9)$$

where the first sum extends only over those degrees of freedom (i_k) of the fluid (i) which are *not* in LTE.

Chemical processes

As was the case for the radiative modelling, detailed chemical modelling is needed for two distinct reasons: (i) to interpret observations (e.g. mass spectra), and (ii) to ascertain the influence of the chemical processes on the coma hydrodynamics. If a reaction involves species belonging to distinct fluids, it will have to be represented by r.h.s. terms in the governing equations of these fluids: an example would be ion–electron recombination reactions in models where ions and electrons make-up separate *fluids (see note 11). In the* innermost coma, however, it is possible to group most *reactive species into the main fluid* (H_2O with trace molecules). The conservation equation for the concentration n_s of a species (s) taking part in N_R reactions involving N_p other products of the same fluid is:

$$\frac{\partial n_s}{\partial t} + \frac{1}{r^2}\frac{\mathrm{d}}{\mathrm{d}r}(r^2 n_s V_i) = \sum_{s'=1}^{N_R} (\nu_{ss'} K_{s'}(T_i) n_1^{m_{ss'}} n_2^{m_{ss'}} \cdots n_{N_p}^{m_{ss'}}) \qquad (10)$$

in which $\nu_{ss'}$ is the stoichiometric coefficient (positive or negative), $K_{ss'}$ the reaction rate, and $m_{ss'} = \sup(\nu_{ss'}, 0)$ the reaction order. The photodestructive reactions which trigger the chemical reactivity can be cast into the preceding form, but with rates which depend upon position r, owing to the strong UV absorption of the coma.

A chemical model suitable for a pure H_2O coma requires consideration of about 100 reactions involving about 20 chemical species, for which the reaction rates are usually (but not always) known. It predicts the gradual enrichment of the coma in H, OH, H_2, O, and O_2, and the gradual development of an ionosphere in which the dominant ion is initially H_3O^+, as verified by the *in-situ* ion mass spectrometer of the *Giotto* probe.

Insofar as the hydrodynamics of the coma is concerned, the pure H_2O model is probably sufficient to represent properly the effect of the coma chemistry, since the addition of trace species can probably not change the mass, momentum and energy perturbations of the main fluid. Even so, a severe difficulty appears when trying to ascertain the energy perturbation, $\dot{E}_{ch} \equiv \dot{E}_{H_2O,H_2O}$ context: a large fraction of $\dot{E}_{ch}$ *is due to excess energy appearing during the photodestruction of* H_2O under the form of kinetic energy of H atoms. The heating of the fluid (at rate $\dot{E}_{ch}$) is thus essentially due to the thermalization of these fast H atoms. It can be shown (e.g. Mendis *et al*.[5]) that the mean-free path for thermalization of these atoms rapidly exceeds the main fluid characteristic length, as distance to the nucleus

Table 2. Model computations of P/Halley primary molecule abundances. "S1988" refers to the model of Schmidt *et al.*[28] and "G1991" to that of Geiss *et al.*[29]. The numbers indicate the best-fit assumed composition of the gas mixture released by the nucleus, normalized to 100 for H_2O. The first group of molecules is common to the two models, the two last groups are specific to one model.

Model	H_2O	CO	CH_4	CO_2	C_2H_2	H_2CO	NH_3	HCN	N_2
G1991	100	15	1	2	1	3.8	1.5	0.1	0.1
S1988	100	10	2.5	3.75	0.84	2.5	2.5	0.07	0.08

	C_2H_4	C_2H_6	CH_3OH	NO	H_2S
G1991	0.3	0.3	0.8	0.2	0.1
S1988	–	–	–	–	–

	CS_2	C_3H_4	H_2CO_2	CH_3CN	CH_3NH_2
G1991	–	–	–	–	–
S1988	1.25	0.06	0.37	0.2	0.1

increases. Thus the H atoms cannot be included into the H_2O fluid. But they do not make-up either a normal fluid to the extent that the free path for H–H equilibration is also larger than the H density decrease scale. This problem has been solved by various means, with poorly agreeing results (see quick review in Crifo[20]). Perhaps the only safe approach is the direct Monte-Carlo simulation, but the only development along these lines (Hodges[19], see Figure 3) did unfortunately not include an evaluation of $\dot{E}_{ch}$ (see note 12).

If one wants to account for the chemistry of H_2O *plus* trace species, the modelling becomes formidable. One has to introduce arbitrarily *C*-bearing, *N*-bearing, and *S*-bearing unobserved species as hypothetical progenitors of the strange (thus *possibly not significant*) subset of observed species of Table 1 and/or of the chemically unidentified species contributing to *in-situ* mass spectra. The most elaborate model is probably that of Schmidt *et al.*[28], with ≃950 reactions involving 59 neutral and 76 ionized species. Figure 5 shows an example of its capabilities: the best fit shown corresponds to the postulated primary gas composition shown in Table 2. Another interpretation of the same data was made independently by Geiss *et al.*[29], using a different network with 21 neutral and 40 ionized species. Their best fit postulated primary composition is also shown in Table 2. The comparison of these two results suggests that this kind of endeavour *cannot* reliably predict the presence of *any* primary molecule at a predicted abundance of order of 1% or smaller: for instance one cannot distinguish between CS_2 and H_2S as the dominant *S*-bearing molecule. Even, the presence or absence of the *identified* species CH_3OH is indifferent!

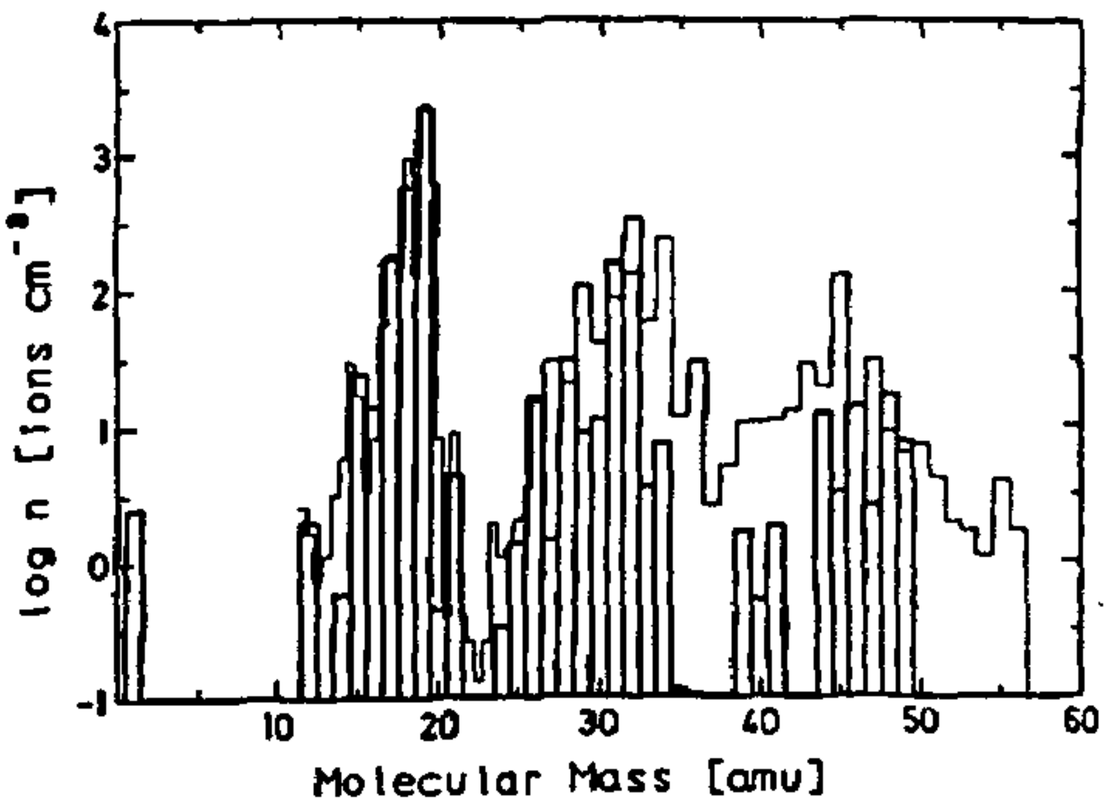

Figure 5. Model fit to P/Halley ion mass spectrum[52]. The thin lines show the ion mass spectrum obtained at 1500 km from the nucleus by the HIS ion spectrometer of the *Giotto* spacecraft, and the heavy lines the best fit obtained with the assumed mixture of primary molecules of Table 2.

Gas–dust interactions

A strong impetus for detailed modelling of the gas-dust interaction has been the determination of the dust grain 'ejection velocity law' $V_d(m_d)$, i.e. of the velocity V_d attained by grains with mass m_d far enough from the nucleus that their interaction with the gas has become negligible. The knowledge of this 'law' is essential to the understanding of the formation of the dust tails, to the assessment of the future of the grains after their ejection (escape from the solar system? incorporation

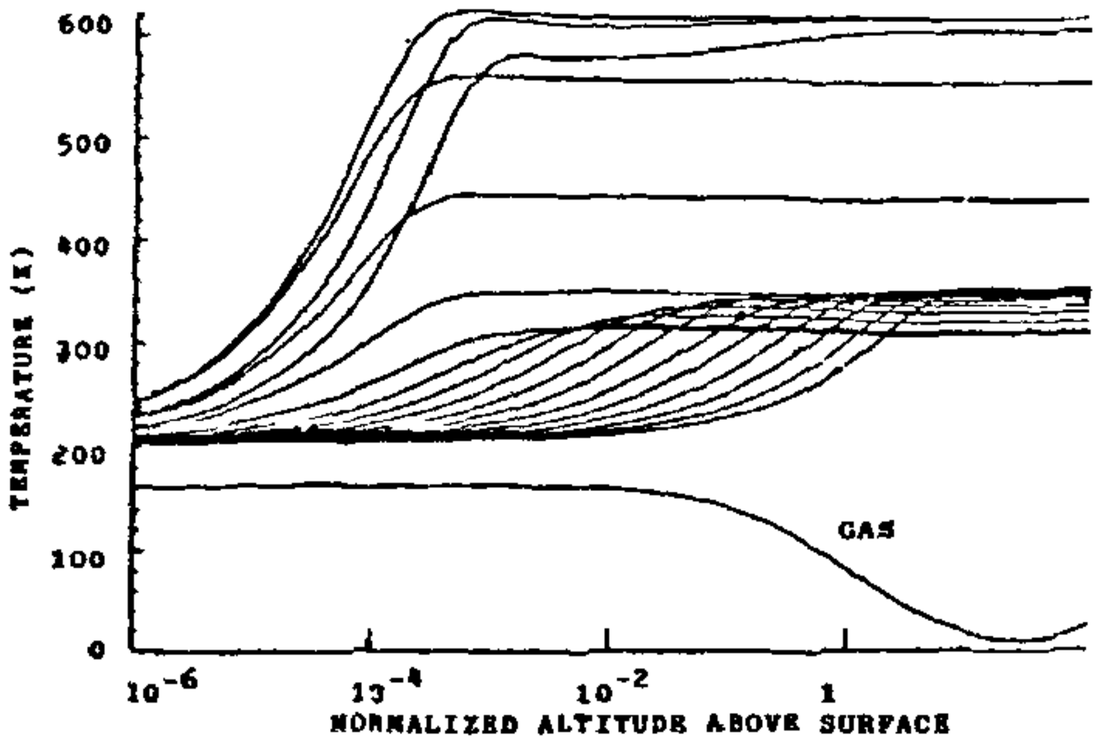

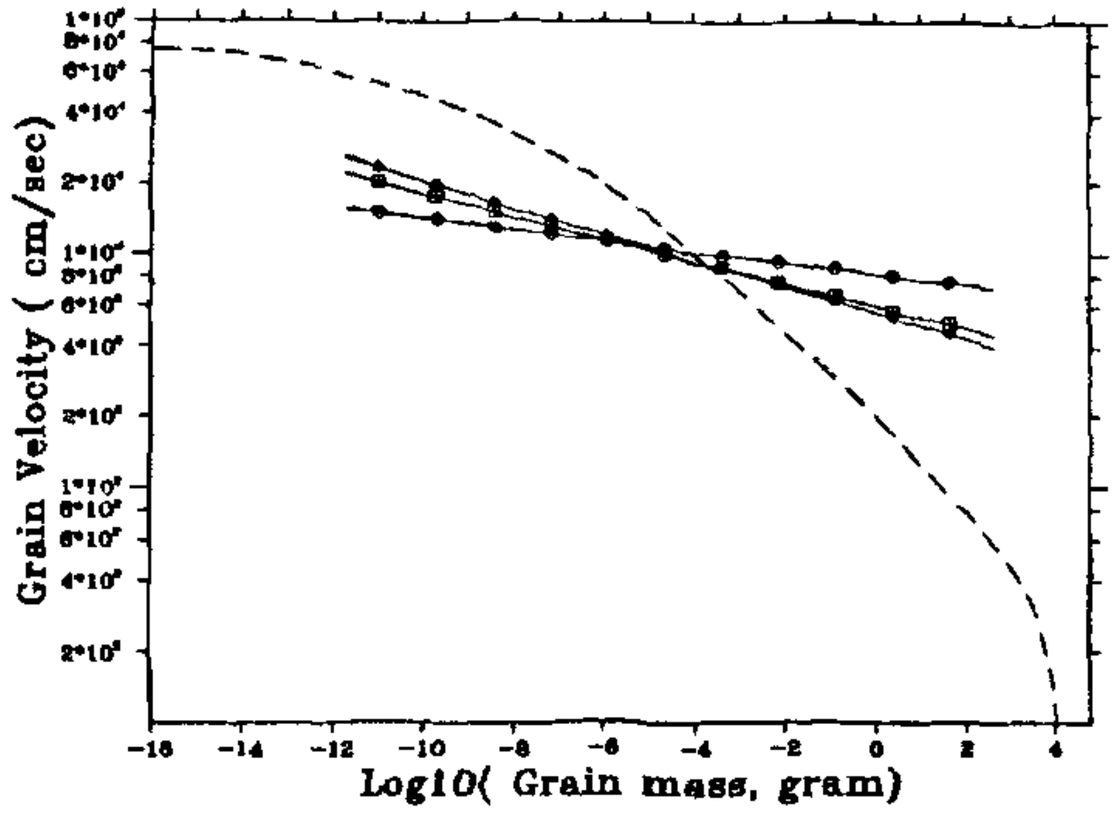

Figure 6. Dust grain velocity and temperature for P/Halley The left panel (from Crifo[20]) shows, as a function of distance to the nucleus, the evolution of the temperature of dust grains with differing sizes (equispaced by factors of 10 in mass) The right panel compares the corresponding computed mass dependence of the *terminal* velocity of the grains (dashed line) with several indirect experimental determinations of dust velocities obtained from dust tail studies[49].

into the zodiacal cloud? into meteor streams?), and also to the evaluation of comet dust mass loss rates. As regards the last point, observations typically provide grain number densities, and to convert these into mass loss rate, one needs to know grain velocities.

The *Giotto* P/Halley flyby mission results have demonstrated that dust grains from fractions of a μm up to at least several mm in size were present in the coma[30]. An estimate of the rates of grain momentum changes due to grain–grain collisions and to gas–grain collisions can be obtained from scaling considerations, and reveals that, for the preceding grain size range, the latter effect is quite dominant. Therefore, the dust grains do not make-up a single fluid, but follow the gas flow (as in a dust storm). Each subset of grains with a common size obeys its own collisionless Boltzman equation with nucleus gravity and gas drag as external forces. One can as well use the moment equations (2)–(4) for each gain size, setting (in view of the absence of grain–grain collisions) $p = T = \mu = \dot{M} = 0$, where T is the grain *kinetic* temperature T – not to be confused with the grain *internal* temperature to be discussed later. Accordingly, equation (4) degenerates into the integral of equation (3), in which the grain–gas momentum exchange term (or drag term) $\dot{\Pi}_{g,d}$ remains to be computed.

Aside from the $V_d(m_d)$, one must compute the evolution of the dust grain internal degrees of freedom, here the dust grain *internal* temperature $T_d(m_d)$. This is needed for the computation of the grain–gas 'convective' energy exchange term $\dot{E}_{g,d}$, and to fit the experimental thermal IR spectra of the dust; T_d is set by the balance between (i) the rate of absorption of solar energy, $E_{abs}(r)$ (see note 13), (ii) the rate of grain thermal energy emission, $\dot{E}_{rad}$, and (iii) the gas–grain exchange term $\dot{E}_{g,d}$:

$$m_d C_d \left(\frac{\partial}{\partial r} + V_d \frac{\partial T_d}{\partial r} \right) = \dot{E}_{abs} - \dot{E}_{rad} + \dot{E}_{g,d}. \qquad (11)$$

For a numerical evaluation of these terms, the utterly simplifying assumption that grains are spherical and homogeneous is made. The radiative terms are then easy to compute in terms of the solar flux and of Planck's law at the grain internal temperature, using the Mie absorption cross-sections $Q_{abs}(m_d, \lambda)$.

The terms $E_{g,d}$ and $\Pi_{g,d}$ depend upon the hydrodynamic regime of flow of the gas past the dust. The precedingly indicated interval of grain sizes is well below typical values of the gas mean-free path Λ – even at the surface of an active nucleus: accordingly, the flow of the gas *past the grains* is free-molecular: $\Pi_{g,d}$ and $E_{g,d}$ are given by classical analytic expressions which involve the velocities and temperatures of the two partners (see, e.g. Mendis *et al.*[5]).

Finally, the non-adiabatic perturbation of the gas outflow induced by the presence of dust is represented, in the gas equations, by the terms:

$$\dot{\Pi}_{d,g} = -\int \dot{\Pi}_{g,d}(m_d)\eta(m_d)\,dm_d;\ \dot{E}_{d\,g} = -\int \dot{E}_{g,d}\eta(m_d)\,d\,m_d \qquad (12)$$

in which $\eta(m_d)$ is the normalized dust mass distribution.

Because observable grains (from the Earth) have sizes comparable to visible and IR wavelengths, it also has long been *assumed* that these sizes were dominant in the comet emission, so that single size dust models were

first developed[5, 25] (note 14). Recently, more realistic models using a large number of size classes have been developed; an example of computed spherical dust grain temperatures and velocities is shown in Figure 6. Although such computed velocities are accepted at large, they are not in particularly good agreement with the indirect information that has been extracted from the modelling of dust tails, as shown by the figure: this is probably a consequence of the assumption of grain sphericity: spherical grains, far from having typical hydrodynamic properties, have indeed very atypical properties (linked to the fact that their external-area-to-volume ratio is minimal): this difficulty persists even though the grains are spinning (see Crifo[21, 36] for a more detailed discussion).

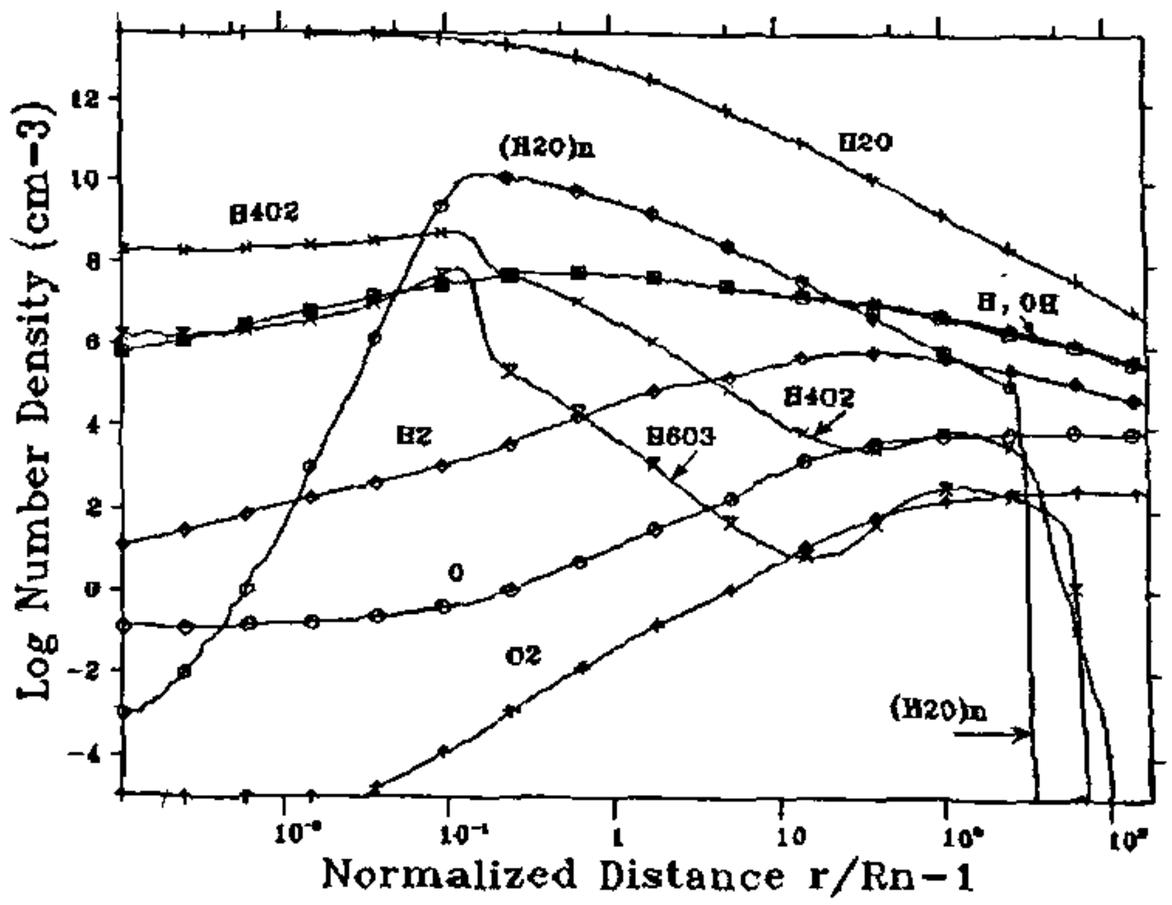

Figure 7. Predicted water recondensation in P/Halley. The figure (from Crifo[33]) shows, as a function of distance to the nucleus surface, the distribution of water and its photodestruction products, plus that of some of the water clusters formed by homogeneous recondensation: the dimer, trimer, and the 'supercritical' clusters $(H_2O)_n$. For the latter, n increases from 7 at the origin, to a peak value of $\simeq 300$ at $\simeq 75$ km from the surface, and decreases beyond this point down to 1 at the point of cluster disappearance, at about 1100 km from the surface.

Water recondensation

The net result of the spherical vacuum outflow of a water-dominated fluid subject to the non-adiabatic processes considered above is, first, a net cooling down to temperatures of order 10 K (e.g. Mendis *et al.*[5]). However, the decrease of the vapour pressure $p_s'(T)$ of H_2O with decreasing temperature is so great that at such temperatures the supersaturation $S = p/p_s$ would attain huge values (much in excess of 10^6!). Such out-of-equilibrium states of a vapour, if indeed reached, would be extremely unstable versus decomposition into a mixture of vapour plus liquid drops (or vapour plus solid flakes). The temperature of the vapour increases as a consequence of this phase separation (or 'partial recondensation'), due to the release of latent heat, and its pressure decreases, due to the condensation, so that S returns to 'reasonable' values in the vicinity of the equilibrium value $S = 1$. The effect can be witnessed in ordinary life (aircraft trails, automobile exhausts,...) and is in frequent use at the laboratory (study of water clusters). Yamamoto and Ashihara[32] were the first to draw attention to it in the case of a comet.

According to the theory of phase separation (initiated by Gibbs at the end of the 19th century, the process occurs via a chain of cluster-forming reactions:

$$X(H_2O)_j + (H_2O) \rightleftharpoons X(H_2O)_{j+1} \quad (j \geq 0) \qquad (13)$$

in which X is a 'condensation center', consisting in a (cold) dust grain, a foreign molecule, an ion, or H_2O itself. Therefore, the modelling of coma water recondensation can be considered as an extension of the modelling of the 'classical' chemical reactivity (see note 15). For large ($\gg 1000$) values of j, the clusters are indeed ice flakes (see note 16).

The first step in the modelling of the effect is the determination of the most efficient condensation centre(s), X. In a coma, dust is an unlikely candidate, because its temperature is raised above that of the gas by solar illumination (see Figure 6). Ions are excellent candidates, but, in the immediate vicinity of the nucleus, the ion density is small, in view of the coma opacity to UV light. Thus, molecules should be considered first, and, in first place, H_2O itself: in such a case, the recondensation is called 'homogeneous'.

The assessment of homogeneous recondensation reaction rates for small values of j is a most difficult task. We refer to Crifo[33] and references therein for the latest developments applied to cometary water: it can be shown that, to a satisfactory approximation, the net budget of the chain of reactions (13) for $X \equiv H_2O$ is the sudden apparition at $r = r_{min}$ very close to the nucleus surface of a concentration n_c of clusters with initial small size $j_c \simeq 7$ (see Figure 7). These clusters first grow, up to a distance r_c (of order 100 km for P/Halley flyby conditions), and beyond this point they are resublimated following their heating by solar light. All clusters disappear completely at r_{max} of order 1000 km in the above example. The peak depletion of water occurs at $r = r_c$ and is small ($\simeq 15\%$), but the most important effect is to buffer the coma temperature everywhere above $\simeq 70$ K.

In view of the fact that the recondensation effect is computed to be restricted to the innermost coma ($r \leq 1000$ km), its experimental detection is presently impossible. There is, however, little doubt concerning its occurrence via one or another channel (i.e. one or another X): Crifo[33] has also investigated the 'proton

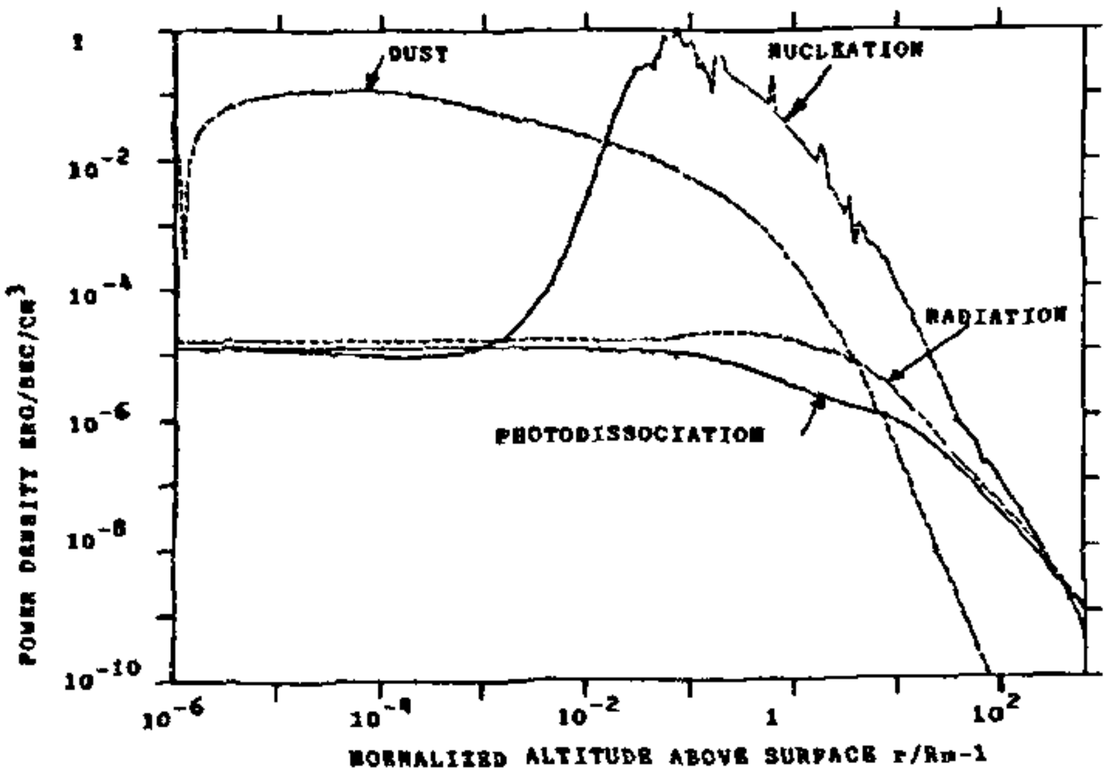

Figure 8. Energy budget of P/Halley's coma[20] Shown as a function of distance to the nucleus surface are the non-adiabatic changes in water energy content due to dust, to radiative effects, to photodissociation, and to recondensation One sees that each of these effects plays a dominant role during some fraction of the history of an outflowing fluid element

hydrates' recondensation channel, for which $X = H_3O^+$, and found that, in the case where the homogeneous channel would not be as efficient as predicted, this proton hydrate route would become an efficient recondensation route.

Conclusion

Comparison between cometary observations and models is currently done on the basis of 'partial' models that put emphasis on one or a few specific effects (e.g. chemistry, radiation, . . .). However, fully convincing conclusions could only come from a global model. Just as an example, we show in Figure 8 the relative importance of the non-adiabatic energy inputs into a spherical pure water coma. One sees that any one of the effects considered precedingly is dominant during some period of the history of an outflowing fluid element, so that the observable coma will bear imprints from all of them.

A comprehensive and self-consistent standard model of the fluid region of a comet is far from having appeared yet, even under utterly simplified geometrical assumptions. However, observations that could provide the necessary boundary conditions and use its results also will not appear before the end of this century. Ample time is thus available to bring the existing partial models into forms that will make them usable for a global model. One probably will have to develop approximate analytic forms for the r.h.s. terms of equations (2) to (4) as obtainable from the partial models.

The distribution of collisionless species

Prior to the middle of this century, only trace radicals (C_2, C_3, CN) and dust were known (see Table 1). It was assumed that stable molecules (e.g. C_2N_2) were *outgassed* – not sublimated – by the nucleus and subsequently photodissociated into these radicals. The corresponding estimated outgassing rates were smaller than the presently known H_2O sublimation rate by at least three orders of magnitude (see Table 1). Therefore, collisions were considered to be totally negligible in the observable 'radical' coma ($r/R_n > 10^3$). Thus, cometary observations were first interpreted using a collisionless formalism and, because habits are so hard to eradicate, sometimes continue to be so under circumstances where this is unphysical (as acknowledged by, e.g. Spinrad[34], and by Jewitt[35]). In many cases, however, the outermost gas coma of all comets is indeed collision-free, and so are the dust tail and, almost always, the dust coma.'

The collisionless effusion of particles (molecules or grains) emitted from a point source in a constant force field (as liquid water in a fountain) has been modelled by Bessel and applied first by him to cometary dust in 1836: it is now in this case called the 'fountain model'; it has been applied to gas much later (in the 1960s) and is referred to in this case as the 'Haser model'. This theoretical field is presently very active, with both analytic and Monte-Carlo approaches being used.

The first step in computing the density of a collisionless population consists in finding the trajectories (usually two) which connect the observational point $\mathbf{r}_h$ to previous cometary orbital positions $\mathbf{r}'_0$ (a so-called Lambert problem) and in computing the corresponding initial velocities $\mathbf{V}'_0(r'_0)$ of particles which follow these trajectories; the d.f. at $\mathbf{r}_h$ is just the sum of the contributions from each of these families of particles:

$$f(\mathbf{r}_h) = \sum_i f(\mathbf{r}'_0) J_i \, e^{-\tau_i} \tag{14}$$

in which τ_i allows for possible destructive effects during the particle travels and is related to the particle radial velocity V'_r and destruction rate β_{ph} by:

$$\tau_i = \int_{r'_i}^{r_h} \frac{\beta_{ph}(r)}{V'_r(r)} \mathrm{d}r, \tag{15}$$

and where the J_i's are the Jacobians

$$J_i = \frac{\partial(\mathbf{r}', \mathbf{V}')}{\partial(\mathbf{r}'_0, \mathbf{V}'_0)}. \tag{16}$$

Values of $\beta_{ph}(r = 1\ \mathrm{AU})$ for gas species are given in Table 1 (see note 17). For inert dust, $\beta_{ph} = 0$ (see note 18).

The computation of J is the second and most difficult task of the problem. A few indications on its computation will be given below.

Neutral particles are submitted in interplanetary space to the solar gravity field $\mathbf{g}_h$:

$$g_h = GM_h / r_h^2 \tag{17}$$

with G the gravitational constant, M_h the Sun mass, and to the solar radiation pressure repulsive force (see note 19) $\mathbf{F}^{pr}$. For molecules and atoms (isotropic scatterers) one has:

$$F^{pr}(r_h, \mathbf{V}) = \sum_l \frac{\pi e^2}{m_e c} f_l \frac{L_h(\nu_l - \frac{\mathbf{V}\cdot\mathbf{r}_h}{c}\nu_l)}{4\pi c r_h^2}, \tag{18}$$

in which the ν_l's are the frequencies of the optical absorbing transitions, the f_l's their oscillator strengths, and L_h the sun luminosity at ν_l (erg cm^{-3} s^{-1}); Doppler shifts have been introduced because of the presence of strong lines in the solar spectrum. For spherical dust grains (see note 20) one has:

$$F^{pr} = \pi a^2 \int \frac{Q_{pr}(a,\nu) L_h(\nu)}{4\pi c r_h^2} d\nu = \pi a^2 \langle Q_{pr}(a)\rangle \frac{E_\odot(r_h)}{c} \tag{19}$$

in which Q_{pr} is the Mie radiation pressure efficiency, a the grain radius, $E_\odot$ the total solar energy flux, c the speed of light, and $\langle\ \rangle$ denotes the solar flux-weighted average.

Thus, in a solar-centered reference frame, molecules and grains move on conical sections in an apparent solar gravity field usually denoted (after Bessel) by $\mu m g_h$ or by $(1-\beta_{pr})\, m g_h$.

For a spherical solid with specific mass ρ_d, one obtains, using equations (17) and (19)

$$\beta_{pr}(a, \rho_d) = \frac{3}{4}\frac{\langle Q_{pr}(a)\rangle}{a\rho_d}\frac{E_\odot(1)}{GM_h c} \simeq 5.95\ 10^{-5}\frac{\langle Q_{pr}\rangle}{a\rho_d} \tag{20}$$

$\langle Q_{pr}\rangle$ varies considerably with grain radius and grain composition. Typical values are $\ll 0.1$ for grains $\ll 0.1\ \mu$m, and $\simeq 1$ for grains $\gg 0.1\mu$m.

For molecules and atoms, β_{pr} is generally negligible: for instance, it is $\simeq 10^{-4}$ for O, $\simeq 10^{-3}$ for C, and $\simeq 1.17\ 10^{-2}$ for OH. It is however nearly equal to 1 in the case of H (see note 21).

In the vicinity of the nucleus, the comet gravity field $\mathbf{g}_c$ must also be considered. In view of the completely non-spherical shape of the nucleus, it varies from point to point on the surface, and is non-central. One has:

$$g_c(\mathbf{r}) = \frac{GM_n}{r^2} + \frac{3G}{2r^4}\left(\sum_1^3 I_j - 3I(\mathbf{r})\right) + \cdots \tag{21}$$

where the I_j's are the three principal moments of inertia of the nucleus, and $I(\mathbf{r})$ its moment of inertia about the direction $\mathbf{r}$. Finally, the grains are submitted to the gasdynamic force imparted by the escaping gas $\mathbf{F}^{gas}$; one has approximately:

$$\mathbf{F}^{gas} = \dot{\mathbf{P}}_{g,d} / n_d \simeq (1/2)\langle C_d\rangle\langle A_d\rangle \rho_g (\mathbf{V}_g - \mathbf{V})^2 (\mathbf{V}_g / V_g) \tag{22}$$

in which $\langle C_d\rangle$ and $\langle A_d\rangle$ are the spin-averaged grain drag coefficient and cross-section, and ρ_g and $\mathbf{V}_g$ the gas density and velocity (see note 22). In writing equation (22), we have assumed that the gas-dynamic spin-up of the grains is fast and that the transverse (lift) force is negligible with respect to the drag. For a spherical outflow at a constant velocity V_g^0 of molecules with molecular mass $\mathcal{A}_g$ sublimated from an effective sphere of radius R_n^{eff} of ice with latent heat $\mathcal{L}_s$ and visible albedo $\mathcal{A}_v$, one has:

$$\mathbf{F}^{gas} \simeq \frac{\langle C_d\rangle}{2}\pi a^2 \mathcal{A}_g V_g^0 \frac{(1-\mathcal{A}_v)\, E_\odot(r_h)}{\mathcal{L}_s}\left(\frac{R_n^{eff}}{r}\right)^2. \tag{23}$$

If we call $\mathbf{r}_h$ and $\mathbf{r}_h^0$ the particle and nucleus position (Sun-centered frame), and $\mathbf{r} = \mathbf{r}_h - \mathbf{r}_h^0$ the comet-centered particle position, one has for a particle of mass m the comet-centered general equation of motion:

$$\frac{d^2\mathbf{r}}{dt^2} = \mathbf{g}_h(\mathbf{r}_h) - \mathbf{g}_h(\mathbf{r}_h^0) + \mathbf{g}_c(\mathbf{r}) + \frac{\mathbf{F}^{gas}(\mathbf{r}) + \mathbf{F}^{pr}(\mathbf{r}_h)}{m} \tag{24}$$

One can expand the r_h-dependent terms in powers of $\mathbf{r}$ around $\mathbf{r}_h^0$ as:

$$\frac{d^2\mathbf{r}}{dt^2} = \mathbf{g}_c(\mathbf{r}) + \frac{\mathbf{F}^{gas}(\mathbf{r})}{m} - \beta_{pr}\mathbf{g}_h(\mathbf{r}_h^0) + (1-\beta_{pr})\mathbf{r}:\nabla_h\mathbf{g}_h(\mathbf{r}_h^0) + \cdots \tag{25}$$

The two first terms represent forces which operate in the vicinity of the nucleus and decay with characteristic scales R_n and R_n^{eff}: they can be dominant only in the so-called circumnuclear region. The third and fourth terms are due to solar gravity and radiation pressure. The fourth term is of order (r/r_h^0) and is therefore important only at very large distances from the comet (dust tail and H coma). The third term – a uniform field – is dominant at intermediate distances, i.e. in the dust and radical coma, except for those species which have a negligibly small β_{pr}.

The circumnuclear region

In this region, by definition, the gas-dynamic force and nucleus gravity are dominant. The dynamics of (collisionless) molecules and of grains are quite different because of their differing mass.

The gas molecules quit the nucleus with velocities much greater than the nucleus escape velocities: therefore, collisionless molecules follow straight lines.

Dust grains assume at the surface of the nucleus thermal velocities which are negligible with respect to the escape velocity. They however are accelerated by molecular impacts (see note 23). The ratio of the nucleus gravity to the gas-dynamic force they undergo is initially independent from r. This ratio is unity at a size a_{max} given, from equations (21) and (23) by[8]:

$$a_{max}(r_h)\rho_d \simeq \frac{3}{8}\langle C_d\rangle \mathcal{A}_g V_g^0 \frac{(1-\mathcal{A}_v)E_\odot(r_h)}{\mathcal{L}_s}\frac{(R_n^{eff})^2}{GM_n}. \quad (26)$$

For P/Halley, this is, in g cm^{-2} $\simeq 28/r_h^2$, with r_h in AU (see note 24). Grains much larger than a_{max} cannot leave the surface. It is easy to compute that grains much smaller than a_{max} are accelerated beyond V_{esc} within a fraction of R_n from the surface; beyond this point, they follow the gas streamlines (if any) until they uncouple from it; their velocity can possibly reach the local gas velocity (very fine dust), but in general levels off at only a fraction of it (see Figure 6).

What happens to grains with $a \simeq a_{max}$ is complex, because in this case the non-sphericity of the nucleus and of the grains, the nucleus rotation, and the localized nature of the gas production must be carefully taken into account[36]. A preliminary numerical investigation of their behaviour has been made by Banaszkiewicz *et al.*[37]. It has revealed the existence of tightly spiralling trajectories for which the grains reside for very long times (weeks at $r_h \simeq 1$ AU) in the vicinity ($r < 80$ km) of the nucleus. Conceivably, then, a comet recessing from the Sun can be surrounded by a halo of initially very large grains (boulders!) gradually enriched in smaller and smaller solids.

What happens at large heliocentric distances ($r_h > 10$ AU) has not yet been studied. For large grains, in equation (25) only the first and last term (with $\beta_{pr} = 0$) will be significant. Long-lived orbits are possible within the distance r_{Hill} at which these two terms become comparable. One obtains:

$$r_{Hill} \simeq r_h^0\left(\frac{M_n}{2M_h}\right)^{1/3} \simeq R_n\left(\frac{\rho_n}{2\rho_\odot}\right)^{1/3}\frac{r_h}{R_\odot} \quad (27)$$

in which $\rho_\odot$ is the Sun specific mass (1.41 g cm^{-3}). Since the solar radius $R_\odot$ equals 1/215 AU, r_{Hill}/R_n is about equal to $200\, r_h$, if r_h is expressed in AU. This means that distant comets can be surrounded by a rather large cloud of grains. Indeed, at least one comet of this kind has been observed (comet Bowell 1980b).

The dust coma

In this region, the dominant force is the solar radiation pressure which can be approximated by a constant field, the third term of equation (25). Its outer extension is at most a fraction of AU, say 0.1 AU.

The inner limit of this region is the outer limit of the circumnuclear coma. Combining equations (19) and (23), one sees that the gasdynamic force dominates the radiation pressure force up to a distance r_{circ} given by:

$$r_{circ} \simeq R_n^{eff}\sqrt{\frac{\langle C_d\rangle}{2\langle Q_{pr}\rangle}\frac{\mathcal{A}_g c V_g^0}{\mathcal{L}_\odot}} \simeq 70\, R_n^{eff}\sqrt{\frac{\langle C_d\rangle}{\langle Q_{pr}(a)\rangle}}. \quad (28)$$

Surprisingly, r_{circ} is independent from heliocentric distance! Only grains smaller than a_{max} travel in this region. Let us call $V_d^0(a)$ the 'terminal' velocity of such a gain: formally speaking, it is its velocity are r_{circ}, but numerical integration of the gas acceleration indicates that it is essentially attained much closer to the surface (say within a few R_n^{eff} from it. Therefore, one can consider that, for a given a, the grain trajectories are those of particles emitted at constant velocity (see note 25) from a point source and in a constant field of force, i.e. parabolas (see Figure 9). One can show (see e.g., Mendis *et al.*[5]) that the *envelope* of the parabolas is *also* a parabola with apex on the comet-to-Sun axis at a distance $L_{pr}/2$ given by:

$$L_{pr}(a, \rho_d, r_h) = \frac{(r^h V_d^0(a, \rho_d, r_h))^2}{2\beta_{pr}(a, \rho_d)\, g_h(1)}$$

$$= 7.1\ 10^3 \frac{a\,\rho_d (V_d^0(a, r_h))^2}{\langle Q_{pr}(a)\rangle}(r_h^{AU})^2. \quad (29)$$

For the observable dust coma (grains in the micron size range) L_{pr} is in the range 10^4 to 10^5 km at 1 AU. The sunward oblate shape of these envelopes is responsible for the current appearance of the dust coma on the solar side of the comet.

The dust density is zero outside of the parabolic envelope; inside, it must be obtained from equations (14) and (16). It can be shown that *for any given* V_d^0 any point within the parabolic envelope corresponding to V_d^0 can be reached by grains travelling along *two distinct* parabolic trajectories (see Figure 9): one parabola (defined by the angles θ_+^0 and ϕ_+^0 at the origin) corresponds to direct access, and the other parabola (θ_+^0 and ϕ_+^0) to access after turn-back of the particle by the radiation pressure (quite like for water drops in a fountain). The distribution function at the origin can be written as:

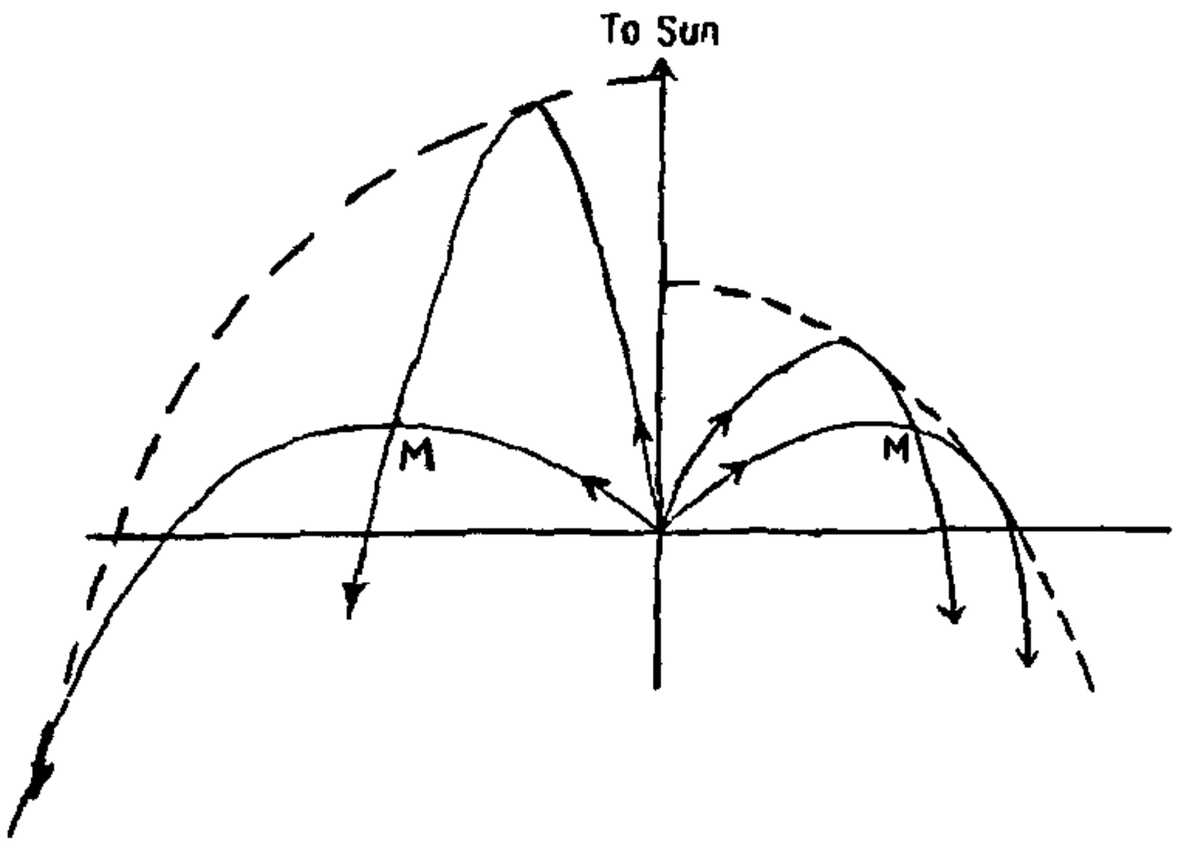

Figure 9. Trajectories of single-size dust grains in a coma. The left and right halves of the figure show dust grain trajectories corresponding to the same grain mass, but to differing ejection velocities V_d^0 : for each V_d^0, one sees that the same point M can be reached along two trajectories as long as M lies within the envelope corresponding to V_d^0 (dashed curve).

$$f^{0}(\mathbf{V}_d^0) = \frac{Q_d(a)}{V_d^0} u(V_d^0, \theta, \phi), \tag{30}$$

where u (cm^{-1} s steradian^{-1}) is the nucleus-averaged dispersion in dust velocity and surface emission rate (resulting from nucleus inhomogeneity and grain shape dispersion), and Q^d the rate of emission (grain/second/cm^2). The Jacobians J_+ and J_- corresponding to the two trajectories are given by[38]:

$$J_{\pm}(a,\ \rho,\ x) = \frac{1/2\rho}{\sqrt{|1-2x'-\rho'^2|}\sqrt{1-x' \mp \sqrt{|1-2x'-\rho'^2|}}} \tag{31}$$

in which ρ is the distance of the point to the comet-Sun axis, and x the abscissa of the point measured along this axis, and $x' = x / L_{pr}$, $\rho' = \rho / L_{pr}$. Finally, the dust number density is given by:

$$n_d(a,\ \rho,\ x) = \int \frac{Q_d(a)}{V} (J_+ u(V, \theta_+, \phi_+) + J_- u(V, \theta_-, \phi_-))\, dV \tag{32}$$

In primitive models, one assumes isotropic production and neglects ejection velocity dispersion: u has then the degenerate form $\delta(V - V_d^0)/4\pi$ which makes the integrations equations in (32) trivial:

$$n_d(a, \rho, x) = \frac{Q_d}{4\pi V_d^0}(J_+ + J_-) = \frac{Q_d}{4\pi V_d'^0 r^2} \frac{1-x'}{\sqrt{1-2x'-\rho'^2}}. \tag{33}$$

However, such a degeneracy induces a divergence in f at the dust envelope. Therefore, it is more convenient to replace the δ function by a Gaussian velocity dispersion with adjustable width ΔV_d^0 when f is to be computed near the envelope (see Beard[38]).

Finally, let us indicate that, if the dust is sublimating or condensing, the preceding expressions must be amended: as a changes, the trajectories are not any more parabolas. This problem has been investigated by Schwehm and Kneissel[39] and by Crifo and Emerich[40] and will not be discussed here.

The collisionless gas coma

The distribution of collisionless molecules can be treated as that of dust, except that photodestructive effects must be introduced. Therefore, in equation (32) one must perform the substitution $Q_d \to Q_g, V_d^0 \to V_g^0$ and $J_\pm \to J_\pm e^{-\beta_{ph} t_\pm}$ in which t_+ and t_- are the easily computable[38] transit times along the two parabolas. Furthermore, u is now a Maxwell–Boltzman function at the nucleus temperature T_n (see note 26). However, the use of equation (32) is unnecessary, because, for most molecules emitted from the nucleus, the range against photodissociation, L_{ph}, is much smaller than L_{pr}. It is easy to show that, in this case:

$$n^p(r) = \frac{Q^p}{4\pi r^2 V^p} e^{-r/L^p} = \frac{Q^p}{r^2 \sqrt{8\pi k_B T_n / m^p}} e^{-r/L^p}. \tag{34}$$

On the other hand, most long-lived species are produced in the photodissociation of one or several parent molecules, and in such a case the preceding formalism must be abandoned (see note 27). An elementary expression for the density n^d of daughter species can be easily derived[40a] in the ideal case where (i) there is only one mother molecule, (ii) this mother molecule is released from the nucleus, (iii) the daughter molecule preserves the velocity vector of the parent molecule, and (iv) the parent and daughter destruction scale lengths L_{ph}^p and L_{ph}^d are much smaller than the corresponding L_{pr}^p and L_{pr}^d's:

$$n^d(r) = \frac{Q^p}{4\pi V^p r^2} \frac{L_{ph}^d}{L_{ph}^p - L_{ph}^d} (e^{-r/L_{ph}^p} - e^{-r/L_{ph}^d}) \tag{35}$$

This expression is still, often used to fit coma isophotes and derive scale lengths. However, the resulting lengths lack any meaning, not only when the coma is collisional, but also when any of the preceding assumptions does not hold. This is commonly the case, because the dissociation product receives an excess kinetic energy (often comparable to, or greater than, the parent kinetic energy) under the form of a more or less

Table 3. Simplified photodestruction scheme of H_2O, after Crovisier[42] and Schmidt *et al* [28]. The excess energy is shared between vibrational and (less significantly) rotational excitation of OH (and presumably of H_2), electronic excitation of O, H and OH^+, and kinetic energy of the products (predominantly of the lightest ones: H and e^-) The rates are for Quiet Sun conditions, at 1 AU, and outside of the coma, they of course are affected by differential absorption inside the coma

Wavelength (Å)	Rate (10^{-6} sec^{-1})	Products	Excess energy (eV)
1450–1860 ('1st band')	6 71	$H + OH (X\,^2\Pi)$	
	0 07	$H_2 + O (^1D)$	3 5
1216 (Lyman α)	3 66	$H + OH (X\,^2\Pi)$	
	0.46	$H + OH (A\,^2\Sigma^+)$	3 4
	0 42	$H_2 + O (^1D)$	3 5
	0 04	$H_2 + O (^1S)$	
≤ 1450 ('2nd band')	0 72	$H + OH (X\,^2\Pi)$	
	0 09	$H + OH (A\,^2\Sigma^+)$	3 4
	0 09	$H_2 + O (^1D)$	3 5
	0 09	$H + H + O (^3P)$	
≤ 980	0 33	$H_2O^+ + e^-$	12 3
	0 013	$H^+ + OH + e^-$	24 9
	0 055	$H + OH^+ + e^-$	18 5
		$H_2^+ + O + e^-$	
	0 006	$H_2 + O^+ + e^-$	36 3

isotropic velocity increase, **W**. Furthermore, **W** is usually spread in magnitude according to some probability distribution $\Phi(W)$. Festou[41] has derived an exact expression for n^d in such a case, valid for a spherically symmetric distribution n^p:

$$n^d(r) = \beta_{ph}^{p} \iiint \left(\frac{r'}{s}\right)^2 n^p(r')\Phi(W)\left(\frac{V}{W}\right)^2 e^{-s/L^d} \times \sin\phi \, d\phi \, dr' \frac{dV}{V} \quad (36)$$

in which:

$$s = \sqrt{r'^2 + r^2 - 2 r r' \cos\phi}$$

$$W = \sqrt{V^2 + (V^p)^2 - 2 V V^p \cos\varepsilon}$$

$$\sin\varepsilon = (r/s) \sin\phi.$$

These expressions constitute part of the so-called vectorial model (see note 28). In practice, of course, $\Phi(W)$ must sum the contributions of each of the competing photodestructive paths leading from the parent to the daughter. It is also possible, in principle, to sum the contributions from several parent molecules. One of the essential difficulties is to find or to guess the corresponding molecular data. The best (yet far from fully) understood and most important case is the photodestruction network of H_2O which we summarize in Table 3.

Sophisticated models of the emissions from the H and from the OH coma have been constructed, from which most of our knowledge of the H_2O production rate is derived. For OH, these models are based either on the vectorial model, or on Monte-Carlo simulations of the distribution of the daughter species[43]. We give some consideration to the case of the H coma in the next subsection. The emissions from more exotic species, in particular CN, C_2, NH_2, have also been investigated in detail; for such cases, the emphasis is placed on the molecular physics of the emission more than on the dynamics of the species, because the origin of these species is uncertain. A spectacular example of successful interpretation of the high-resolution spectrum of a minor species in nearly pure fluorescent equilibrium is the recent work of Gredel *et al.*[44] on C_2.

The atomic H coma and the dust tail

Atomic hydrogen results from the photodissociation of H_2O and its daughter OH; owing to its small mass, it carries away most of the excess kinetic energy of the dissociation, its excess velocity being in the range $V_H \simeq$ (1 to 25) km/s. Combined with its small destruction rate β_{SW} (Table 1) (see note 29), this gives survival distances $L^H \simeq$ (0.15 to 3) 10^8 km (or 0.1 to 2 AU!).

The dust grains are not photodestructed, therefore they travel across a large fraction of the Solar System: indeed, typical dust tail lengths are of order of fractions

of AU (see note 30). In the context of the present oversimplified dust models, dust grains are spherical and leave the nucleus with a mass-dependent velocity V_d (m_d) smaller than the gas velocity, i.e. of order of fractions of km/s.

Thus, the dynamics of the H coma and of the dust tail bear close similarities. Their modelling requires the full use of equations (14), (15) and (16). One must first understand why the former make-up a *nearly spherical* coma, while the latter make-up a tail.

We now consider an ecliptic coordinate system, and take the collisional coma as a point source, considering the characteristic dimension of the present problem. A typical cometary nucleus velocity (within 1 AU) is $V_n \simeq 50$ km/s, not much greater than V_H, but much greater than V_d^0. Therefore, the dust grains *initial* velocity distribution is nearly $\delta(\mathbf{V} - \mathbf{V}_n)$; consider all the grains ejected *at a given time* t_0: they describe Kepler orbits all situated *in the comet orbital plane*, all initially tangent to $\mathbf{V}_n$ (t_0), but gradually divergent from one another because of the mass dependence of the force $\mu m \mathbf{g}_h$ (equations (17) to (19)). At a later time, t, the grains which have differing masses are separated from one another: the locus of their positions defines a curve called a *synchrone*. As exemplified in Figure 10, the dust distribution formed by the *successive* synchrones corresponding to successive times t_0 within a certain interval Δt_0 of peak dust emission (say, the vicinity of the perihelion) has the roughly antisolar fan-like appearance characteristic of dust tails.

If, on the other hand, the size distribution of the *observable* grains is narrow, the synchrones are only a narrow segment: the tail resembles more the so-called *syndyne* (or *syndyname*), which is the locus, *at a given instant* t, of the positions of the grains of a given mass that left the comet at *all* earlier times (see Figure 10).

For a detailed fit of tail images, it is necessary to allow for the spread in grain trajectories introduced by the grain ejection velocity V_d^0. This was done in first-order approximation by Finson and Probstein[25]: they assumed that all grains of a given mass m_d, and emitted at the same time t_0, instead of being at a later time t at the same position $\mathbf{r}_0$ (m_d, t_0, t), as if V_d^0 (m_d) = 0, in reality are distributed over a sphere centered at this point, and with radius $\Delta = V_d^0(m_d)(t - t_0)$. The synchrones and syndynes, accordingly, become 'pencils' with radius Δ. In this way, the Lambert problem is avoided, but the accuracy of the assumption is uncertain.

In the case of the H atoms it is not at all possible to represent the initial velocity by a δ function: in orientation, it is not very different from isotropy (it has only a 'bump' in the direction of $\mathbf{V}_n$); and in absolute value, it has a broad width resembling the sum of Maxwellians (each dominant path in Table 3 giving one

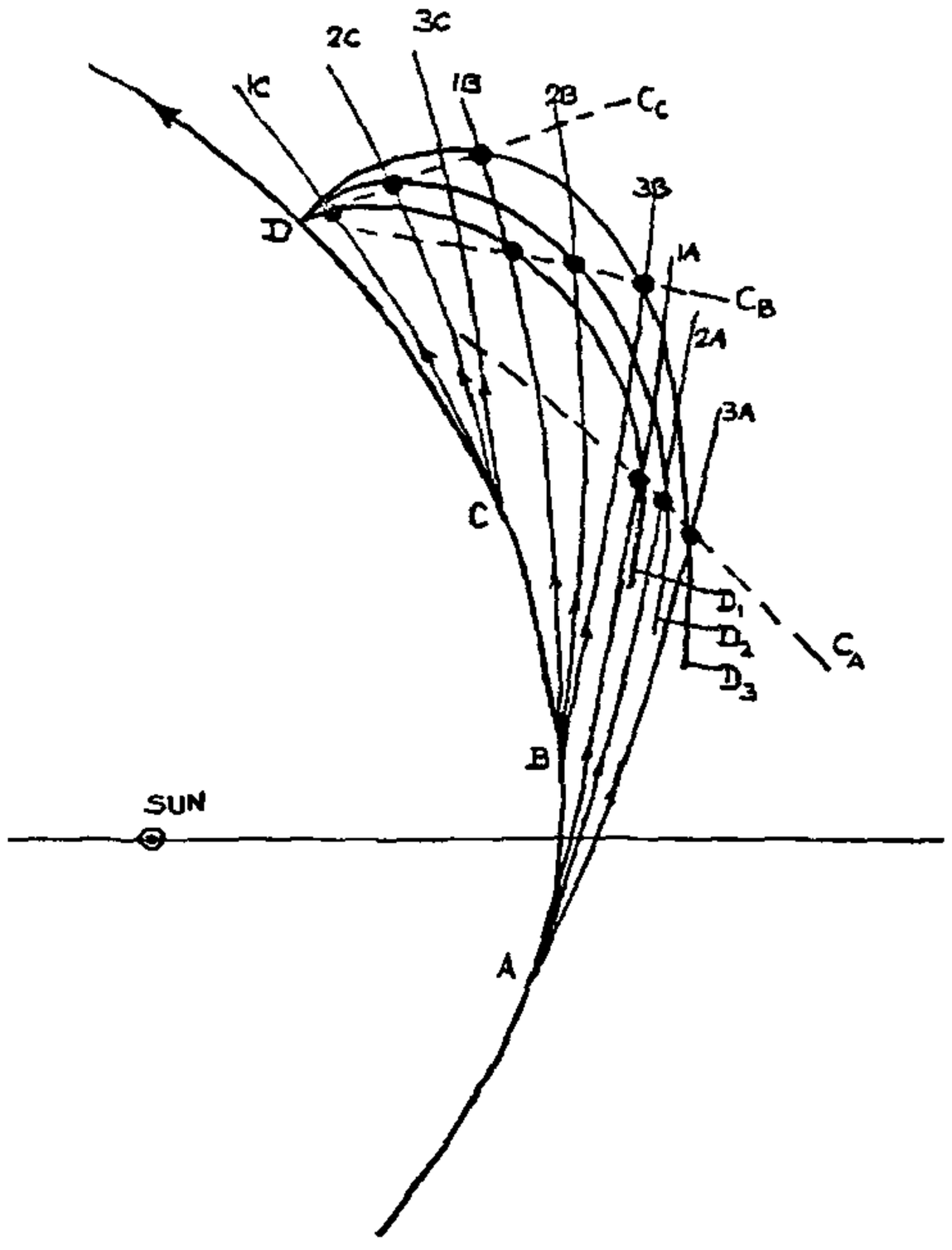

Figure 10. Syndynes and synchrones for a comet. The situation is represented at time t, where the comet is at C(t). The trajectories (1, 2, 3) of grains with three differing masses m_i (i = 1, 2, 3), having left the comet at times t_a (a = A, B, C) are shown, together with the positions of these nine grains at time t (big dots). The synchrones C_a (left) connect the positions of the grains with a common emission time t_a, and the syndines D_i (right) connect those of the grains with a common mass m_i.

term of the sum). Thus, the comet-orbital plane and direction of motion do not play a dominant role in shaping the distribution of H. Furthermore, there is no mass-dispersion effect. If we neglect the complication that μ is time and velocity dependent, the synchrones are now not any more pencils, but large surfaces resembling spheroids. The syndyne concept, although sometimes used, is of little interest because, now, strictly speaking, the syndyne is . . . a *volume* (the full H coma!) (see note 31).

The mathematical modelling of dust tails and H comas based on *exact* particle trajectories is in full development presently (1991). Two differing approaches are used, both aimed at the evaluation of equation (14). The first approach consists in first solving numerically the Lambert problem, and then computing analytically the Jacobian (equation (16)). It was developed for the H coma by Ashihara[45] and for the dust tail by Richter and Keller[46]. The second approach is a

Monte-Carlo simulation developed, for the H coma, by Kitamura *et al.*[47] and Combi[48], and for the dust coma by the Trieste group (see Fulle *et al.*[49] and references therein). In both cases, one of the main difficulties yet to be solved is the derivation of reliable initial velocity distributions: in the case of the dust, this is tied to the uncertain validity of the simplifying assumptions introduced to solve the gas–dust interaction (see Crifo[36]); in the case of the H atoms, it is linked to the multiplicity of the water destruction paths and to the incomplete thermalization of the H atoms.

Conclusion

No quantitative model fit of the atmosphere of any comet has ever been achieved. However, it is clear from the numerous successful partial fits of specific cometary phenomena that the processes which govern the aeronomy of comets are now well understood: the absence of global model is due to the absence of appropriate input boundary conditions, i.e. to the lack of knowledge of the properties of the nucleus. Certainly, the methods developed to model coma processes do not resemble much classical planetary aeronomy tools. But the basic physics, the basic chemistry, the dominant chemical species, and even the current physical conditions in a coma are very familiar. What then is the ultimate reason for the 'strangeness' of comets which is so evident for the observer as well as for the model builder? It would seem that this is simply the complete dominance of solar heating over nucleus gravitational binding. Thinking about comets should therefore induce us into thinking also about the fragility of planetary atmospheres close to a star, and, as a specially important case, about the fragile evolutionary sequence that, in the early times of the Solar System, has allowed the formation of our terrestrial atmosphere.

Note added in proof (January 1994): Comets are really never disappointing: in July 1992 an unknown comet passing by Jupiter was tidally disrupted into a string of at least 20 separate pieces forming a spectacular object now called comet Shoemaker-Levy. This strange object is presently orbiting Jupiter, and expected to rush into the planet by July 1994, forming a series of gigantic explosions. See papers by Chapman, *Nature*, 1993, **363**, 492 and by Melosh and Schenk, *Nature*, 1993, **365**, 731.

1 Grewing, M., Praderie, F. and Reinhardt, R (eds), *The Exploration of Halley's Comet*, Springer, Berlin 1987, (first printed as *Astron Astrophys*, Vol. 187)
2. Mason, J W. (ed), *Comet Halley· Investigations, Results, Interpretations*, Ellis Horwood, New York, 1990, 2 volumes
3 Bailey, M E, Clube, S V. and Napier, W. M., *The Origin of Comets*, Pergamon, 1990
4. Newburn, R. L. Jr, Neugebauer, M. and Rahe, J (eds), *Comets in the Post-Halley Era*, Kluwer, Dordrecht, 2 volumes, 1991
5. Mendis, D. A., Houpis, L. F. and Marconi, M L., *Fundam Cosmic Phys*, 1985, **10**, 1–380.
6. Schoemaker, E. M. and Wolfe, R. F., in *Satellites of Jupiter* (ed Morrison, D), Univ. of Arizona Press, 1982, pp 277–339
7. Meech, K. J., *Physical Aging in Comets* (ref 4), 1991, vol 1, pp 629–669
8. Whipple, F. S, *Astrophys. J.*, 1950, **111**, 375–394
8a. Whipple, F. S., *Nature*, 1976, **203**, 36–49
9 Weaver, H. A, Mumma, M. J. and Larson, H P, *Infrared Investigations of Water in Comet P/Halley* (ref 1), 1987, 411–418.
10. Krankowski, D. and 11 co-authors, *Nature*, 1986, **312**, 326–329
11. Moroz, V. and 16 co-authors, *The Detection of Parent Molecules in Comet P/Halley with the IKS Vega Experiment* (ref 1), 1987, pp. 513–518.
12 Newburn, R L. Jr and Spinrad, H, *Astron J*, 1989, **97**, 552–569
13. Hughes, D. W, *Possible Mechanisms for Cometary Outbursts* (ref. 4), 1991, pp 825–851
14. Belton, M. J S., Julian, W H., Anderson, A. J and Mueller, B E. A., *Icarus*, 1991, **93**, 183–193
15. Peale, S. J, *Icarus*, 1989, **82**, 36–49.
16. Sekanina, Z., *Cometary Activity, Discrete Outgassing Areas, and Dust Jet Formation* (ref 4), 1991, pp 769–823.
17. McCourt, F. R. W., Beenakker, J. J M, Köhler, W E and Kuscer, I., *Nonequilibrium Phenomena in Polyatomic Gases*, Clarendon Press, Oxford, 1990.
18. Crifo, J. F., *Astron Astrophys*, 1989, **223**, 365–368.
19 Hodges, R. R, *Icarus*, 1990, **83**, 410–433
20. Crifo, J. F., *Hydrodynamic Models of the Collisional Coma* (ref 4), 1991, pp 937–989
21 Körösmezey, A. and Gombosi, T I, *Icarus*, 1990, **84**, 118–153
22. Kitamura, Y., *Icarus*, 1990, **86**, 455–475
23. Shimizu, M., *Astrophysics. Space Sci.*, 1976, **40**, 149–155.
24. Crovisier, J, *Astron. Astrophys*, 1984, **130**, 361–372.
25. Finson, M L. and Probstein, R. F., *Astrophys J.*, 1968, **154**, 327–380.
26. Cravens, T. E., *Plasma Processes in the Inner Coma of Comets* (ref 4), 1991, pp. 1121–1255
27. Chin, G and Weaver, J. A., *Astrophys J.*, 1984, **285**, 858–869
28 Schmidt, H U., Wegmann, R., Huebner, W F. and Boice, D C, *Comp Phys Comm.*, 1988, **49**, 17–59
29. Geiss, J. and 8 co-authors, *Astron Astrophys.*, 1991, **247**, 226–234.
30. McDonnell, J A. M., Lamy, P. L. and Pankiewicz, G. S, *Physical Properties of Cometary Dust* (ref 4), 1991, pp. 1043–1074.
31. Salo, H, *Icarus*, 1988, **76**, 253–269.
32. Yamamoto, T. and Ashihara, T., *Astron Astrophys*, 1985, **152**, L17–L20
33 Crifo, J. F, *Astrophys J*, 1992, **391**, 336–352
34 Spinard, H, *Am Rev. Ast Astrophysics*, 1987, **25**, 231–269
35. Jewitt, D, *Cometary Photometry* (ref 4), 1991, pp 19–65
36. Crifo, J F, *In-situ Doppler Velocimetry of very large grains*, ESA report SP-328, Paris, 1992, pp 65, 70
37. Banaszkiewicz, M., Marconi, M, Kömle, N I and Ip, W H, MPAE preprint, Lindau (RFA), 1989.
38. Beard, D. B., *Astrophys J.*, 1981, **245**, 743–752
39. Schwehm, G and Kneissel, B, *Optical and Physical and Dynamical Properties of Dust Grains*, ESA report SP-174, Paris, 1981, pp 77–84.
40. Crifo, J. F. and Emerich, C, in *Ices in the Solar System* (eds Klinger, J *et al*), D. Reidel, Dordrecht, 1985, pp 429–442
40a. Haser, L, *Bull. Acad R Belgique*, 1957, **43**, 740
41. Festou, M, *Astron. Astrophys*, 1981, **95**, 69–79
42. Crovisier, J., *Astron Astrophys*, 1989, **213**, 459–464
43 Bockelée-Morvan, D, Crovisier, J. and Gérard, E, *Astron Astrophys.*, 1990, **23**, 382–400.

44 Gredel, R., van Dischoek, E. F. and Black, J. H., *Astrophys. J.*, 1989, **338**, 1047–1070.

45 Ashihara, O., A theoretical determination of the density at a travelling source that emits particles, ISAS RN, 351, Tokyo, 1986.

46 Richter, K. and Keller, H U., *Astron Astrophys*, 1987, **171**, 317–326

47. Kitamura, Y, Ashihara, O and Yamamoto, T., *Icarus*, 1985, **61**, 278–295.

48 Combi, M R, *Astrophys. J.*, 1988, **327**, 1026–1043 and 1043–1059.

49. Fulle, M, Cremonese, G, Jockers. K. and Rauer, H, *Astron. Astrophys.*, 1992, **253**, 615–624

50 Keller, H U. and 21 co-authors, *Comet P/Halley's Nucleus and its Activity* (ref 1), *1987*, pp 807–823.

51 Bockelée-Morvan, D and Crovisier, J., *The 2 ^{7} m Water Band of Comet P/Halley* (ref. 1), 1987, pp. 425–430

52 Wegmann, R., Shmidt, H. U., Huebner, W. F and Boice, D. C., *Cometary MHD and Chemistry* (ref. 1), 1987, pp. 339–350.

Notes

1. In the following, '*x* AU' means 'at an heliocentric distance of *x* *times the mean* Sun–Earth *distance* of $\simeq 1.5\ 10^{8}$ km'

2 As noted by Whipple[8a] himself, this *idea* had been advanced earlier, but he was the first to consider it seriously.

3. Beyond this distance, most of the solar energy is reradiated under the form of nucleus infrared thermal emission.

4. It is almost certain that the group of the 16 so-called Kreuz Sun-grazing comets were formed in the disintegration of a mother comet with nucleus size $\simeq 100$ km; several other comets are also considered as having common progenitors. A most recent *splitting* event is that of comet P/Chernykh in mid-April 1991

5. Although confusion in this respect is frequent in the literature, if one wants to introduce an 'effective' spherical radius for a (highly nonspherical) comet nucleus, one must give it *differing* numerical values depending on whether one wants to represent the gravity, the active area size, or any other property.

6 The gravitational trapping of a cloud of dust is in principle possible but in absence of gas emission (see 'The circumnuclear region section)

7 It is perhaps useful to recall that the *correct* expression for Λ in terms of the gas number density n_g is $1/(n_g \sigma_g \sqrt{32})$.

8 As H atoms, electrons are produced with velocity excesses, and their incorporation into a single fluid is not necessarily a good approximation

9 Thereafter, we assume that the constituents which are not in equilibrium are however not too far from it, so that they constitute a 'transition regime' fluid This may however not be applicable to H in *the intermediate coma.*

10 We can only mention here the pioneering 2-dimenstional and 3-dimenstional models of the circumnuclear region of Körösmezey, A and Gombosi, T. I [21] and of Kitamura[22].

11 The assessment of reaction rates between species not in thermal equilibrium is in this case, a source of difficulty

12 The problem of modelling the distribution of the H atoms arises also in the context of interpreting the Lyman α emissions from the Huge H coma we give a brief overview of it in section 'The atomic H coma and the dust tail'

13 E_{abs} depends upon r in the vicinity of the nucleus, due to the attenuation of solar light by the dust grains themselves This effect is usually not very strong see Salo[23]

14 These authors derive the gas velocity and *the* dust velocity $V_d(a_d, r_{d\,g})$ for a spherical nucleus emitting *single size* spherical grains with radius a_d and responsible for a fraction $r_{d\,g}$ of the total comet loss. Their solutions have been subsequently used – improperly – to represent the dust velocity *dispersion* in the case where $r_{d\,g}$ is due to a large interval of dust radii.

15. The 'classical' chemistry is due to the establishment of covalent or ionic bonds, whereas the formation of molecular clusters is due to 'Van der Waals' bonds – for water, H-bonds.

16 Ice flakes form below the triple point, 273.1 K for water, and *liquid drops above it*

17. β_{ph} is generally due to UV light and is therefore time-dependent. The values given generally refer to Quiet Sun conditions Furthermore, the contribution of discrete solar emission lines, especially Lyman α, is often dominant, so that β_{ph} can become velocity-dependent, due to Doppler shifts. For H atoms, the leading destructive effect is the interaction with the Solar Wind, not the photodestruction.

18 The case of 'active' dust (i e., sublimating or pyrolizing hot dust, but also possibly accreting *cold icy grains)* is more complex: in this case, a changes with position, therefore, instead of a β_{ph}, one must define a rate of mass change $Z(m) = (1/m)\,|\,dm/dt\,|$.

19. Other forces of radiative origin, e g the Poynting-Robertson drag and the Yarkovski effect are negligible on the time scale of cometary studies; such is not necessarily the case of the electromagnetic forces resulting from photoelectric charging of dust grains, but we omit them here.

20. By 'grain' we mean any solid from submicron to decimeter size! There is no reason why they should be spherical However, because they are expected to be randomly spinning in general, their average optical properties are close to those of 'effective' spheres with radius $a \simeq \sqrt{\langle A_g \rangle / \pi}$ where $\langle A_g \rangle$ is the orientation-averaged cross-section.

21. For H, μ and β_{pr} furthermore vary with solar activity because the radiation pressure is due predominantly to UV transitions for which L_α varies with time.

22. Equation (22) holds irrespective of whether the gas is in free-molecular or in collision-dominated regime, but the numerical value of $\langle C_d \rangle$ depends upon it.

23 One has here to assume that the fraction of molecules scattered by collisions on dust is negligible with respect to those which escape freely.

24. This estimate corresponds to $\mathcal{A}_\mu \ll 1$ and to a free-molecular drag coefficient for spheres $\langle C_g \rangle \simeq 3$ A dispersion in grain shape would result in a tremendous dispersion in a_{max} values (see Crifo[16]).

25. Here, we follow the simple approach initially introduced by Bessel and developed by Eddington If grains were spherical indeed, I_d^0 *would indeed be function of* a *alone* But for aspherical grains, the grain shape is an essential factor also (see Crifo[16]) One can allow for this by introducing a velocity dispersion parameter ΔI_d^0.

26 At a local point of the nucleus surface, u is a *half space* Maxwellian, at a distance $r \gg R_n$, the velocity is aligned onto the direction *from the nucleus, and its dispersion is given by a* Maxwellian at T_n, if – more realistically – there is a temperature variation on the nucleus surface, u will vary with θ and ϕ through T_n

27 The case of H will be discussed separately below

28 The full model includes in addition heuristic algorithms intended to allow for the existence of a *collision dominated* region for the parent molecule

29 β_{sw} is due to electron impact ionization and to proton charge exchange Strictly speaking, the latter effect is akin to scattering more than to destruction, but the *newborn H atoms are* so fast that their resonance Lyman α transition is Doppler-shifted away from the Solar line

30 The 'tail length' is a purely observational concept the tail brightness decreases with dust number density, but also with distance to the Sun and to the Earth, and scattering phase angle. Part of the dust can sometimes even escape from the Solar System

31 Authors usually still define a syndyne *curve* as the locus of H atoms emitted with $V_H = 0$ This does not represent a useful approximation to realistic V_H, but provides a rough estimate of the 'position' of the H coma